SANDIA REPORT
SAND2009-6831
Unlimited Release
Printed September 2009

High Fidelity Nuclear Energy System Optimization Towards an Environmentally Benign, Sustainable, and Secure Energy Source

David E. Ames II, Pavel V. Tsvetkov, Gary E. Rochau, Salvador Rodriguez

Prepared by
Sandia National Laboratories
Albuquerque, New Mexico 87185 and Livermore, California 94550

Sandia is a multiprogram laboratory operated by Sandia Corporation,
a Lockheed Martin Company, for the United States Department of Energy's
National Nuclear Security Administration under Contract DE-AC04-94AL85000.

Approved for public release; further dissemination unlimited.

Sandia National Laboratories

Issued by Sandia National Laboratories, operated for the United States Department of Energy by Sandia Corporation.

NOTICE: This report was prepared as an account of work sponsored by an agency of the United States Government. Neither the United States Government, nor any agency thereof, nor any of their employees, nor any of their contractors, subcontractors, or their employees, make any warranty, express or implied, or assume any legal liability or responsibility for the accuracy, completeness, or usefulness of any information, apparatus, product, or process disclosed, or represent that its use would not infringe privately owned rights. Reference herein to any specific commercial product, process, or service by trade name, trademark, manufacturer, or otherwise, does not necessarily constitute or imply its endorsement, recommendation, or favoring by the United States Government, any agency thereof, or any of their contractors or subcontractors. The views and opinions expressed herein do not necessarily state or reflect those of the United States Government, any agency thereof, or any of their contractors.

Printed in the United States of America. This report has been reproduced directly from the best available copy.

Available to DOE and DOE contractors from
U.S. Department of Energy
Office of Scientific and Technical Information
P.O. Box 62
Oak Ridge, TN 37831

Telephone: (865)576-8401
Facsimile: (865)576-5728
E-Mail: reports@adonis.osti.gov
Online ordering: http://www.osti.gov/bridge

Available to the public from
U.S. Department of Commerce
National Technical Information Service
5285 Port Royal Rd
Springfield, VA 22161

Telephone: (800)553-6847
Facsimile: (703)605-6900
E-Mail: orders@ntis.fedworld.gov
Online order: http://www.ntis.gov/help/ordermethods.asp?loc=7-4-0#online

SAND2009-6831
Unlimited Release
Printed September 2009

High Fidelity Nuclear Energy System Optimization towards an Environmentally Benign, Sustainable, and Secure Energy Source

D. E. Ames[1], P. V. Tsvetkov[1], G.E. Rochau[2], S. Rodriguez[2]
[1]Texas A&M University, 129 Zachary Engineering Center, College Station, TX 77843-3133
[2]Sandia National Laboratories, P.O. Box 5800, Albuquerque, NM 87185-0748

Abstract

The impact associated with energy generation and utilization is immeasurable due to the immense, widespread, and myriad effects it has on the world and its inhabitants. The polar extremes are demonstrated on the one hand, by the high quality of life enjoyed by individuals with access to abundant reliable energy sources, and on the other hand by the global-scale environmental degradation attributed to the affects of energy production and use. Thus, nations strive to increase their energy generation, but are faced with the challenge of doing so with a minimal impact on the environment and in a manner that is self-reliant. Consequently, a revival of interest in nuclear energy has followed, with much focus placed on technologies for transmuting nuclear spent fuel.

The performed research investigates nuclear energy systems that optimize the destruction of nuclear waste. In the context of this effort, nuclear energy system is defined as a configuration of nuclear reactors and corresponding fuel cycle components. The proposed system has unique characteristics that set it apart from other systems. Most notably the dedicated High-Energy External Source Transmuter (HEST), which is envisioned as an advanced incinerator used in combination with thermal reactors. The system is configured for examining environmentally benign fuel cycle options by focusing on minimization or elimination of high level waste inventories.

Detailed high-fidelity exact-geometry models were developed for representative reactor configurations. They were used in preliminary calculations with Monte Carlo N-Particle eXtented (MCNPX) and Standardized Computer Analysis for Licensing Evaluation (SCALE) code systems. The reactor models have been benchmarked against existing experimental data and design data. Simulink®, an extension of MATLAB®, is envisioned as the interface environment for constructing the nuclear energy system model by linking the individual reactor and fuel component sub-models for overall analysis of the system. It also provides control over

key user input parameters and the ability to effectively consolidate vital output results for uncertainty/sensitivity analysis and optimization procedures.

The preliminary analysis has shown promising advanced fuel cycle scenarios that include Pressure Water Reactors Pressurized Water Reactors (PWRs), Very High Temperature Reactors (VHTRs) and dedicated HEST waste incineration facilities. If deployed, these scenarios may substantially reduce nuclear waste inventories approaching environmentally benign nuclear energy system characteristics. Additionally, a spent fuel database of the isotopic compositions for multiple design and control parameters has been created for the VHTR-HEST input fuel streams. Computational approaches, analysis metrics, and benchmark strategies have been established for future detailed studies.

ACKNOWLEDGMENTS

This paper is based upon work supported through the Excellence in Engineering Research Program by the Sandia Research Graduate Program at Texas A&M University and the College of Engineering, Texas A&M University.

INTENTIONALLY LEFT BLANK

CONTENTS

ABSTRACT 3
ACKNOWLEDGEMENT 5
CONTENTS 6
FIGURES 7
TABLES 8
NOMENCLATURE 10
1 INTRODUCTION 13
2 BACKGROUND 17
2.1 The Nuclear Fuel Cycle 17
2.2 Advanced Fuel Cycle Initiative 18
3 OBJECTIVES 20
4 PROCEDURES 21
4.1 Nuclear Energy System Setup 21
5 APPLIED CODE SYSTEMS 23
5.1 Code Systems 23
6 SYSTEM PARAMETERIZATION AND REPRESENTATIVE MODELS 25
6.1 Reactor Units 25
6.1.1 AP1000 25
6.1.2 Model Description 26
6.1.3 Benchmark Analysis 30
6.1.4 VHTR 31
6.1.5 Model Description 32
6.1.6 Benchmark Analysis 40
6.1.7 High-Energy External Source Transmuter 43
6.1.8 External Neutron Source Survey 44
6.1.9 Model Description 44
6.2 Fuel Cycle Components 45
6.2.1 Front-End Components 45
6.2.2 Reprocessing - Partitioning/Separation 48
6.2.3 High Level Waste Storage Facility 48
6.3 Integrated Model 48
7 Preliminary Results 50
7.1 AP1000 50
7.1.1 Neutronic Analysis 50
7.2 VHTR 54
7.2.1 Neutronic Analysis: LEU Fuel 54
7.3 AP1000 - VHTR 57
7.3.1 Neutronic Analysis: TRU Fuel 57
7.4 HEST 61
8 CONCLUSIONS 63
8.1 Future Plans 63
9 References 65
10 Appendix A 67

FIGURES

Figure 1.1. Relationship of HDI and Electricity Consumption per Capita. 14
Figure 1.2. HDI vs. CO2 Emissions per Capita for 180 Countries. 15
Figure 4.1. Nuclear Energy System. 22
Figure 6.1. Fuel Assembly. 26
Figure 6.2. AP1000 Reactor Core Map. 27
Figure 6.3. PYREX Rod Arrangement within the Fuel Assembly. 28
Figure 6.4. IFBA Rod Arrangement within the Fuel Assembly. 28
Figure 6.5. Neutron Flux Profiles in the Fuel Rods (MCNP vs. SCALE). 31
Figure 6.6. Prismatic Fuel Block (measurements in cm). 33
Figure 6.7. VHTR Fuel Element. 34
Figure 6.8. VHTR Prismatic Fuel Block. 36
Figure 6.9. Replaceable Reflector Blocks. 37
Figure 6.10. Control Rod Guide Block (measurements in cm). 38
Figure 6.11. VHTR Whole-Core 3D Model Geometry Details. 39
Figure 6.12. Neutron Flux Profiles in the Fuel Rods (MCNP vs. SCALE). 43
Figure 6.13. Prismatic Block with Neutron Source. 45
Figure 6.14. NFCSS Components. 46
Figure 6.15. CAIN Transformation Chain. 47
Figure 7.1. AP1000 Whole Core Depletion with MCNPX Code. 51
Figure 7.2. AP1000 Fuel Rod Spectra for Different Fuel Enrichments. 51
Figure 7.3. AP1000 Production and Consumption of Higher Isotopes in Reference Core. 52
Figure 7.4. Reactivity of LEU-Fueled VHTR. 54
Figure 7.5. LEU-Fueled VHTR Spectra for Core Regions. 55
Figure 7.6. Production and Consumption of Higher Isotopes in LEU-Fueled VHTR. 56
Figure 7.7. TRU-Fueled VHTR Spectra for Core Regions. 58
Figure 7.8. TRU-Fueled VHTR Spectra of Particles, Compacts, and Fuel Blocks. 58
Figure 7.9. TRU-Fueled VHTR and AP1000 Spectra for the Fuel Assemblies. 59
Figure 7.10. Reactivity of TRU-Fueled VHTR. 60
Figure 7.11. HEST Spectrum of the Fuel Block. 61
Figure 7.12. HEST, AP1000, and VHTR Spectra Comparison. 62
Figure 8.1 Integrated Model Flowchart. 64

TABLES

Table 6.1. AP1000 Design Parameters. 26
Table 6.2. Reactor Core Description. 29
Table 6.3. Multiplication Factor Results. 30
Table 6.4. VHTR Design Parameters. 32
Table 6.5. Prismatic Fuel Block Properties. 34
Table 6.6. Fuel Element Properties. 35
Table 6.7. Burnable Poison Rod Properties. 35
Table 6.8 Replaceable Reflector Block Properties. 37
Table 6.9 Control Rod Guide Block Properties. 38
Table 6.10. HTTR Design Specifications. 40
Table 6.11. Results for Different Heterogeneity Treatments. 41
Table 6.12. Experiment-to-Code Benchmark Results. 41
Table 6.13. Basic Reactor Physics (Withdrawn Control Rods). 42
Table 6.14. Code-to-Code Results. 42
Table 6.15 Nuclides Included in CAIN Calculation. 47
Table 6.16. NFCSS Input Parameters. 48
Table 7.1. Nuclide Masses in the AP100 at Different Burnup Levels. 53
Table 7.2. AP1000 TRU Vectors at 40 GWd/MTU. 54
Table 7.3 Nuclide Masses in the LEU-Fueled VHTR at Different Burnup Levels. 56
Table 7.4 Fuel Composition for the TRU-Fueled VHTR. 57
Table 7.5 Fuel Composition for the TRU-Fueled VHTR. 60

NOMENCLATURE

ADS	Accelerator Driven System
AFCI	Advanced Fuel Cycle Initiative
AP1000	Westinghouse Electric Company Reactor
BOC	Beginning of Cycle
CAIN	CAlculation of INventory of spent fuel
CO2	Carbon Dioxide
COLs	Combined Construction and Operating Licenses
CPU	Central Processing Unit
D	Deuterium
DOE	United States Department of Energy
DU	Depleted Uranium
EFPD	Effective Full Power Days
EOC	End of Cycle
FP	Fission Product
GCC	Gulf Cooperation Council
GDP	Gross Domestic Product
Gen. IV	Generation IV Nuclear Fuel Systems
GIF	Generation IV International Forum
HDI	Human Development Index
HEST	High-energy External Source Transmuter
HLW	High Level Waste
HTGR	High Temperature Gas Reactor
HTTR	High Temperature Test Reactor
IAEA	International Atomic Energy Agency
IFBA	Integral Fuel Burnable Absorber
JAERI	Japan Atomic Energy Research Institute
LEU	Low Enriched Uranium
LLW	Low Level Waste
LWR	Light Water Reactor
MCNPX	Monte Carlo N-Particle eXtented
MTU	Metric Ton Heavy Metal
NES	Nuclear Energy System
NFCSS	Nuclear Fuel Cycle Simulation System
NGNP	Next Generation Nuclear Plant
NRC	United States Nuclear Regulatory Commission
ORNL	Oak Ridge National Laboratory
OTTO	Once Through Then Out
PWR	Pressurized Water Reactor
PYREX	Discrete Burnable Absorber Rods
SCALE	Standardized Computer Analysis for Licensing Evaluation
SWU	Separative Work Unit
T	Tritium
TRISO	TRIstructual ISOtropic coated fuel particles
TRU	Transuranic Isotopes (Np, Pu, Am, Cm)

UNDP	United Nations Development Program
UQ	Uncertainty Quantification
UREX	URanium EXtraction
VHTR	Very High Temperature Reactor

INTENTIONALLY LEFT BLANK

1 INTRODUCTION

It is difficult to describe how important energy has become in the world today. Industrialized nations are totally dependent on an abundant reliable supply of energy for living and working, and it is a key ingredient in all sectors of modern economies. Even so, it is often taken for granted because it plays such a large role in everyday existence. Meanwhile, in developing countries there is almost an unquenchable thirst for substantial increases in energy generation and usage. In any case, energy is one of the single most important factors in regards to living standards of individuals across the world. Studies have continually shown an indisputable link between energy consumption and individuals overall well being [1-3].

Large amounts of data have been collected for comparing average energy consumption per capita to measurements that represent the standard of living or quality of life achieved in any community. One such measure is the Human Development Index (HDI) [2], which incorporates factors such as life-expectancy, education, income inequality, poverty rates, Gross Domestic Product (GDP) per capita, and the environment.

The HDI is widely considered to be the best and most comprehensive measure for quality of life. The index is normalized to give a value between zero and one, with one representing the highest possible standard of living or most developed country, and zero being the least. Countries that score an HDI greater than 0.90 are considered to have a “very high quality of life”, while those with values between 0.60 and 0.90 are rated as having an “average quality of life”, and those below 0.60 are classified as having a “very low quality of life.”

A very compelling relationship is that of HDI and energy usage. The data presented in Figure 1.1 was released by the United Nations Development Program (UNDP) on December 20, 2008. It includes the HDI and electricity generation per capita (as determined in 2006) for 180 different countries, with some of the countries labeled for general reference. As indicated, the results overwhelmingly show that the greater the energy consumption per capita for a community the greater the standard of living (HDI) for those individuals. Consequently, energy consumption can be used as a litmus test for the overall well being of a society and for a comparison between different societies around the globe.

Iceland and Norway have the highest HDI at 0.968, while Sierra Leone ranks lowest at 0.329. The US has an HDI of 0.950 and is ranked number 15 overall. As expected all nations strive to increase HDI, and the most effective and straight forward way to accomplish this is by adding energy generation capacity. Of particular notice is China and India, the two most populated countries in world, which have HDI values that place them in the lower portion of the “average quality of life” group of nations. As both India and China strive to rapidly increase their HDI it will greatly affect the rest of the world. With over 35% of world’s population between them just a slight increase in either’s electricity consumption per capita will have a huge impact on overall energy needs worldwide.

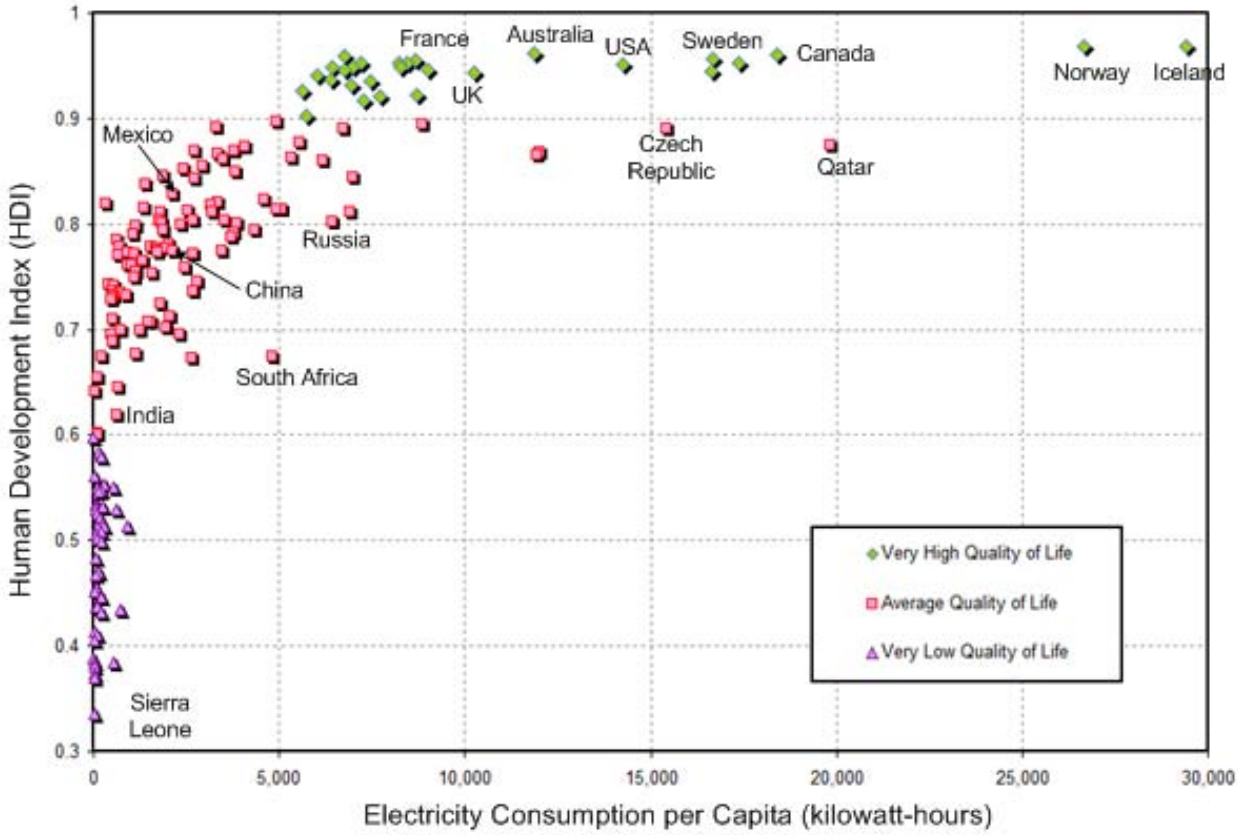

Figure 1.1. Relationship of HDI and Electricity Consumption per Capita.

The coupled affect of energy use and living standards leads to an interesting dilemma. Just like energy's link to quality of life, energy is also intricately entwined with the environment. Much of the global-scale environmental degradation seen today is attributed to the adverse effects of energy production and use. Thus, nations are faced with the struggle to increase energy generation in order to provide a higher standard of living for their citizens, but must also do so in an environmentally responsible way.

Figure 1.2 displays Carbon Dioxide (CO2) emissions and HDI data for 180 countries around the world. The six countries (Bahrain, Kuwait, Oman, Qatar, Saudi Arabia, and the United Arab Emirates) that make up the Gulf Cooperation Council (GCC) are at the top or near the top of the list for CO2 emitters, mainly due to their high emitting gas production sector, small populations, and exportation of energy. Qatar is the number one emitter, generating 79.3 tones/capita - such a high value that it does not even fit on the scale of the provided plot. Many of the GCC countries have taken aggressive measures to reduce CO2 emissions. Including tightening controls on gas flaring, researching carbon capture and sequestration, and investigating the use of non-CO2 emitting energy forms such as nuclear energy and wind power.

It is interesting that counties such as France and Iceland have extremely high HDI values while at the same time generating very low levels of CO2 emission per capita. Further investigation reveals that France gets about 80% of its electricity generation from nuclear power and much of

Iceland's energy needs are met by renewable sources (particularly geothermal power), so both countries are fulfilling a large portion of their energy needs by non-CO2 emitting sources. Iceland and France have something else in common - they both have very few fossil fuel energy resources within their borders. Even so, they have adopted energy plans that have made them much more energy-independent as compared to other industrialized nations.

The US is 9th on the list for CO2 emissions per capita and 2nd, just behind China, for overall CO2 emissions. The rest of the world shares the belief that the US needs to take a more proactive role in CO2 reduction and set an example for the others around world to follow. Again, as mentioned previously, China and India are of major concern due to their large populations and the impact they will have in the future.

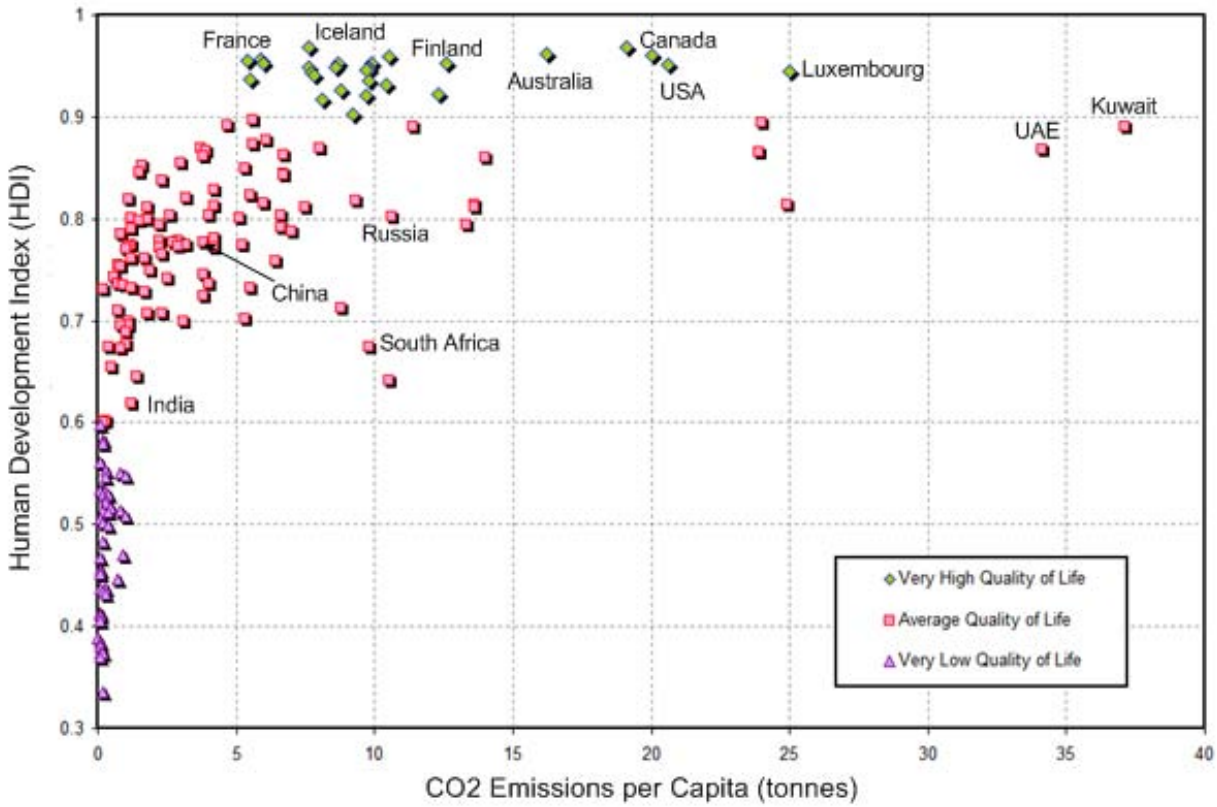

Figure 1.2. HDI vs. CO2 Emissions per Capita for 180 Countries.

Of recent, the world has become much more sensitive to the relationship between energy and the environment, to the point that it has become impossible to discuss one without the other. In response, nations and groups of nations have proposed and/or implemented policies [4, 5] to mitigate the harmful environmental effects associated with energy generation. These energy policies are developed to aid the environment through tactics such as carbon emission caps, emissions trade plans, carbon taxes, efficiency and conservation incentives, clean renewable energy incentives, etc. In addition to the very important environmental issues that have come to the forefront, there are some other important requirements for future energy systems. Important goals and basic principles of future energy sources include:

1) reducing greenhouse gas emissions,
2) minimizing the overall environmental footprint,
3) safety and reliability,
4) sustainability,
5) economics,
6) efficiency, and
7) energy independence.

From the onset nuclear power has shown great promise in meeting all of the above principles. As the technology has matured so has its effectiveness in accomplishing these goals. Today nuclear energy is arguably one of the best sources for electricity generation that can meet future needs and requirements. Even so, advances and improvements must be made for nuclear energy to be competitive in the future. The research work presented within addresses all of the above principals with emphasis on environmental aspects by means of developing a modeling approach for advanced nuclear energy systems that minimize high level waste inventories while at the same time maximizing fuel utilization.

2 BACKGROUND

2.1 *The Nuclear Fuel Cycle*

The nuclear fuel cycle can be described as the comprehensive collection of components that are linked together for the main purpose of generating electricity by means of nuclear power. It includes everything from the exploration for uranium deposits, to harnessing the energy released during fission, to the disposal of radioactive waste. The nuclear fuel cycle can be thought of as the progression of nuclear fuel through a series of differing stages which involve the production of electricity in nuclear reactors. It can be broken down into three major parts: 1) Front-end, 2) In-core, and 3) Back-end.

The front-end of the fuel cycle begins with the exploration of uranium deposits. Estimates for uranium reserves at different stated costs are developed and reported [6]. Once the uranium deposits have been identified the uranium ore is extracted by various mining methods. Conventional techniques such as open pit and underground mining are most commonly used. Next is the milling process, in which mined uranium ore is processed and treated to extract the uranium. The milled uranium is then converted to a form that can be used by commercial facilities to enrich the fissile component by either gaseous diffusion or gas centrifuge enrichment technologies. The last step for the front-end is fuel fabrication, where enriched fuel is converted to a final usable fuel form and incased in a protective cladding for service in nuclear reactors.

The in-core or service period of the fuel cycle makes up the second major category of the fuel cycle. As the name implies, this part of the fuel cycle is concerned with fuel performance while in the reactor core. Much emphasis is placed on fuel management strategies, irradiation effects on the fuel, fuel cladding interactions, and radioactivity release during normal use and accidents. The reactor type, neutron spectrum, and fuel type are important parameters for the service period.

The back-end of the fuel cycle begins when the fuel is discharged from the reactor. Upon removal, the fuel is stored onsite temporarily and then prepared for either permanent storage or for reprocessing. The decision of whether to recycle the used reactor fuel or to place it directly into storage greatly affects the makeup of the back-end of the fuel cycle. Waste management is the key issue with this part of the fuel cycle.

The US employees what is referred to as the once through fuel cycle. The fuel makes one pass through a thermal reactor core and after removal it is prepared for permanent disposal. The cycle is quite wasteful of nuclear energy resources, being that the valuable remaining energy in the used fuel is not reclaimed. For this reason, the once-through cycle is sometimes called a “throw-away” [7] fuel cycle. Due to its wide use, the once through cycle is often used as the standard reference when comparing differing fuel cycles.

2.2 Advanced Fuel Cycle Initiative

Much effort has been put forth with the goal of making improvements to and/or replacing the once-through fuel cycle with a superior method that recycles used nuclear fuel. For instance, the United States Department of Energy (DOE) established the Advanced Fuel Cycle Initiative (AFCI) program to focus on the research and development needed to support a transition from the current once-through fuel cycle to an advanced nuclear fuel cycle. The AFCI program is envisioned to support the growth of nuclear power and enable energy independence in the US by developing and demonstrating technologies that facilitate the transition to a stable, long-term, environmentally, economically, and politically acceptable advanced fuel cycle. The main goals of the AFCI are to reduce high-level waste volume, greatly reduce long-lived and highly radiotoxic elements, and reclaim valuable energy content of spent nuclear fuel. In short, the AFCI program seeks to:

- Reduce the long-term environmental burden of nuclear energy through more efficient disposal of waste materials.
- Enhance overall nuclear fuel cycle proliferation resistance via improved technologies for spent fuel management.
- Reduce the inventories of civilian plutonium
- Enhance energy security by extracting energy recoverable in spent fuel and depleted uranium, ensuring that uranium resources do not become a limiting resource for nuclear power.
- Improve fuel cycle management, while continuing competitive fuel cycle economics and excellent safety performance of the entire nuclear fuel cycle system.
- Develop fuels and fuel cycles for current reactor systems and future Generation IV nuclear fuel systems (Gen. IV)

The Generation IV International Forum (GIF) focuses on future nuclear energy system concepts to meet the growing energy needs of the world. It is an international program consisting of 13 member nations (US, Argentina, Brazil, Canada, France, Japan, South Korea, South Africa, Switzerland, United Kingdom, the European Union, China, and Russia) coordinating research and working together to develop promising new nuclear energy systems. Attention is given to improving safety features, addressing nuclear nonproliferation and physical protection issues, optimizing natural resource utilization, minimizing waste, and being economically competitive with other energy generating systems. The GIF has selected six systems for further development. The systems are:

1) Gas-Cooled Fast Reactor,
2) Very High Temperature Reactor,
3) Supercritical Water Cooled Reactor,
4) Sodium Cooled Fast Reactor,
5) Lead Cooled Fast Reactor, and
6) Molten Salt Reactor.

As part of the Gen. IV program the US DOE has focused efforts on the Next Generation Nuclear Plant (NGNP). The NGNP program promotes research and development specific to the VHTR.

The VHTR is designed to be a high-efficiency system, which can supply electricity and process heat to a wide-range of high temperature and energy intensive applications. The VHTR is a passively safe design. The refractory core, low power density, and low excess reactivity enable this design feature. It is graphite moderated gas-cooled reactor that supplies heat with core outlet temperatures equal to or greater than 850 degree Celsius, which enables applications such as hydrogen production, process heat for the petrochemical industry, or sea water desalination.

To realize the full potential of advanced fuel cycles fast neutron spectrum systems must be implemented. Fast systems offer a higher degree of flexibility when it comes to the transmutation process. They not only provide the ability to better control the isotopic makeup of the waste stream through nuclide destruction, but also the capability to fully utilize the available fuel resources with high conversion/breeding ratios. The GIF recognizes this and has included fast spectrum systems for further development.

In addition to the fast reactors within the GIF framework, subcritical systems with external sources, also called hybrid systems, demonstrate significant promise for energy generation as well as a neutron excess which could be used for nuclear waste transmutation [8-12]. Hybrid systems are generally separated into two general concepts that are relevant to the approach used to generate the external source of high-energy neutrons: 1) The accelerator driven systems, which combines a particle accelerator with a sub-critical core and 2) Fusion-fission systems, which take advantage of an intense high-energy fusion neutron source.

Subcritical systems driven by an external neutron source have the ability to achieve extremely high transmutation efficiencies in a single core loading without recycle [13], thus minimizing the handling and storage of nuclear waste, making hybrids highly efficient relative to other waste reduction schemes. In addition, recent developments and advances in the arena of combining neutron-rich fusion with energy-rich fission has made fusion-fission hybrid systems a waste destruction strategy that is considerably less costly than known alternatives [14].

3 OBJECTIVES

The overall objective of the proposed research is the development of high fidelity nuclear energy system optimization towards an environmentally benign design that is sustainable and provides a secure energy source. System needs and performance requirements that lead to an actinide-free high-level waste assuming partitioning and transmutation will be targeted. The research objectives can be cataloged as follows:

- Development of Realistic Reactor Core Models

  An integral part of the research is the development of high fidelity whole-core 3D exact geometry models accounting for core physics in the fuel cycle analysis. The modeling approach will be limited to technologically feasible configurations and use hybrid Monte Carlo methods. A major constraint on the computational models will be the computational run time.

- Code System Integration

  Develop an approach to seamlessly couple the various models that compose the environmentally benign system. The goal being to devise a computational shell that effectively controls the entire set of reactor and component models with control over key user input parameters and the ability to effectively consolidating vital output results into readily usable form for uncertainty/sensitivity analysis and optimization procedures.

- Uncertainty Quantification (UQ)

  Quantify the uncertainties for specific core characteristics that greatly affect performance with respect to nuclear waste minimization and determine which data contribute the most to uncertainty.

- Optimization Analysis

  High fidelity nuclear energy system multi-objective optimization for minimizing the problematic actinide isotopes as related to long-term repository storage, minimizing used fuel handling issues throughout the process, and at the same time maximizing the efficient use of the fuel component for prolonged usage and sustainability of fuel resources.

- Environmental Impact Analysis

  Demonstrate the effectiveness of the optimized nuclear energy system as related to environmental impact by drawing comparisons to other proposed advanced fuel cycle schemes and the current once-through fuel cycle.

4 PROCEDURES

4.1 Nuclear Energy System Setup

In the context of this paper a Nuclear Energy System (NES) is defined as a configuration of nuclear reactors and corresponding fuel cycle components. There are numerous possibilities for nuclear energy systems, many of which have been studied in great detail. The proposed NES has some unique characteristics that set it apart from other systems. It is arranged for minimization or elimination of high level waste inventories, which is an essential component of publicly acceptable sustainable nuclear energy strategies [15].

The arrangement of the NES is depicted in Figure 4.1. The front-end (mining, milling, enrichment, and fuel fabrication) of the fuel cycle is shown using a faded coloring scheme to set it apart from the rest of the system. This is not because it is less important, but because the performed analysis for the front-end is treated outside the loop of parameter controls and optimization procedures. Instead an analysis of uranium mining needs and resource availability as related to the NES is performed.

Following the front-end procedures the fuel elements enter the PWR for reactor operation and power production. When the fuel is exhausted it is removed from the reactor and temporarily stored to allow the used fuel to cool down to the specified limits required before reprocessing can be performed. During reprocessing the fuel is partitioned into three separate streams: 1. Fission Products (FP), 2. Depleted Uranium (DU), and 3. Transuranics (TRU). The FPs are conditioned and prepared for long-term High Level Waste (HLW) storage. The DU is stored as Low-Level Waste (LLW) and is also available for recycle. The TRUs are fabricated into fuel elements to be recycled in the VHTR, which operates in the Once-Through-Then-Out (OTTO) mode. The fuel is removed from the VHTR once it no longer can sustain criticality. After a decay/cool-down period the used VHTR fuel is sent to the external source driven subcritical reactor, or HEST, where it is transmuted via single pass. After removal the used HEST fuel is considered HLW and sent to the designated facility for permanent HLW storage.

The material is tracked throughout the NES with emphasis on composition changes within the reactor systems, material streams during reprocessing, and the final affect on HLW waste management strategies. The representative models for the reactor systems and fuel cycle components are stand-alone units that also offer the ability to link each for the purpose of NES uncertainty quantification and optimization procedures.

The proposed advanced NES is anticipated to have a high national and international impact, potentially changing nuclear waste management and reactor deployment paradigms by offering an environmentally benign, sustainable, and secure energy source.

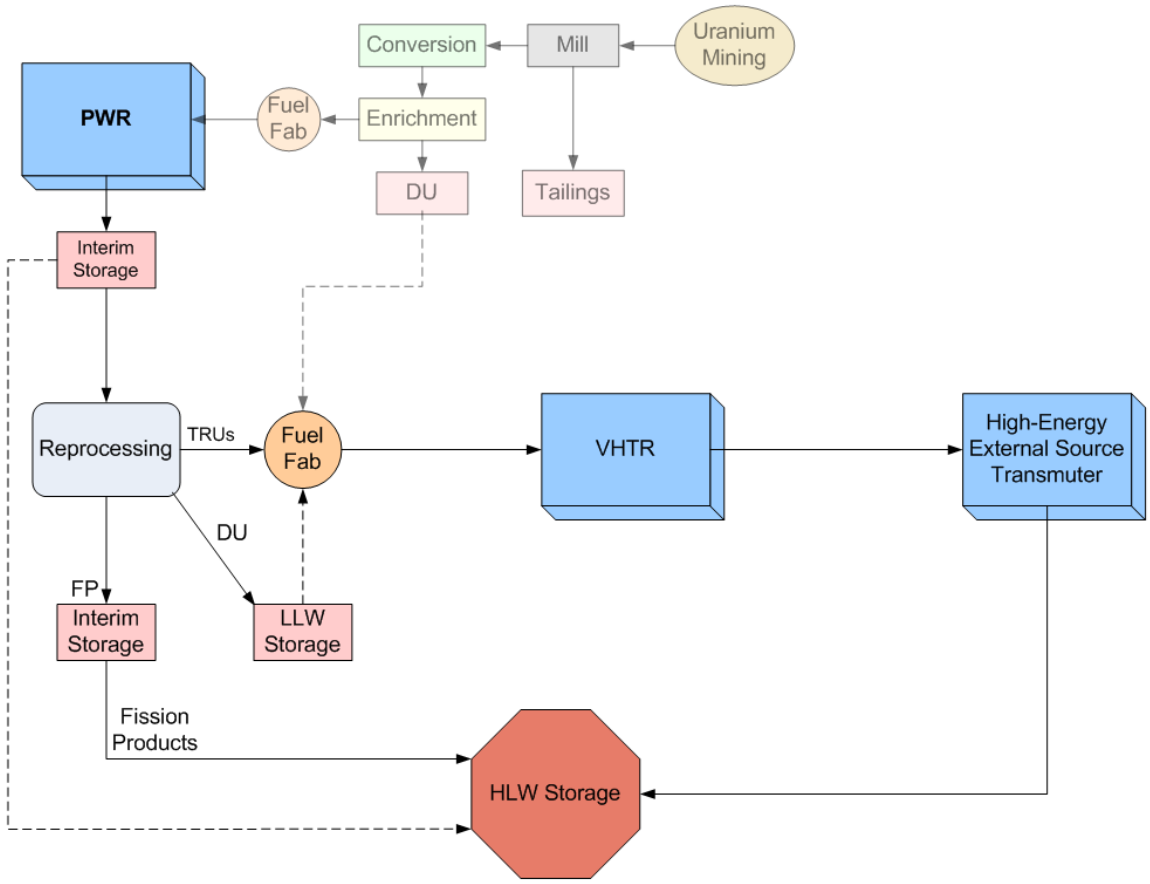

Figure 4.1. Nuclear Energy System.

5 APPLIED CODE SYSTEMS

Modeling and simulation play a critical role in modern scientific and technical endeavors. To the extent that scientific advances are dependent on their effective use. Modeling, theory and simulation can enhance our understanding of known systems, provide qualitative and quantitative insights into experimental work, guide the choice of the experimental system to study, enable the design of new systems, provide quantitative results to replace experiments, and extend limited experimental data into new domains of parameter space [16]. Due to the difficulties of dealing with radioactive materials, modeling and simulation will play a critical role in advancing nuclear research programs.

Most of the available well-established and validated computer code systems are oriented for evaluating light water reactor systems. To apply them for advanced reactor systems a specialized approach of application is required. For instance, previous work [17] has identified insufficiencies in the ability of code systems to accurately account for the multi-heterogeneity effects associated with VHTR systems. Additionally, the modeling of subcritical systems with external sources present challenges involved with accounting for the introduction of a neutron source inside a multiplying media. The neutron kinetic characteristics of subcritical, source-driven cores, as well as the mathematical methods to treat their temporal behavior, are markedly different from those of critical cores [18]. Also, a reliable and consistent procedure for coupling the reactors and other fuel cycle components while preserving and producing key component parameters must be approached with great care.

UQ is a key component for successfully meeting the overall objectives of the proposed research work. UQ is the science of combining imperfect information from multiple sources to reach conclusions and to evaluate the validity of the conclusions. UQ is thus concerned with the transformation from data to knowledge to decisions. It defines the link between science and the decision process. UQ starts with the identification and characterization of error or uncertainties from all steps in the sequence of approximation that leads to a computational model prediction. UQ uses techniques from fields such as statistics and optimization to determine the sensitivity of models to inputs with errors, and to design models in order to minimize the effect of the errors. Integrating uncertainty quantification approaches into simulation allows potentially more efficient interrogation of parameter dependencies and model certainties [19].

5.1 *Code Systems*

State-of-the-art computer code systems are utilized to create realistic high fidelity 3D whole-core models representing the reactors and fuel cycle components that compose the NES. The Monte Carlo code MCNPX [20] is used to construct the reactor models and produce neutronic data for nuclear physics calculations, perform depletion sequences, and provide heat load and dose calculations.

MCNP (Monte Carlo N-Particle) is a general purpose code that can be used for neutron, photon, electron, or coupled neutron/photon/electron transport. MCNPX (Monte Carlo N-Particle

eXtended) extends the capabilities of MCNP to nearly all particles, nearly all energies, and to nearly all applications without an additional computational time penalty. MCNPX is fully 3D and time dependent. It uses up to date nuclear cross section libraries and physics models for particle types and energies where tabular data are not available. MCNPX is a trademark of Los Alamos National Security, LLC, Los Alamos National Laboratory.

The SCALE (Standardized Computer Analysis for Licensing Evaluation) code system [21] serves in conjunction with MCNP to provide code-to-code benchmarking when applicable and for additional analysis beyond that of MNCP. SCALE is developed and maintained by Oak Ridge National Laboratory (ORNL) and is widely accepted around the world for criticality safety analysis.

The International Atomic Energy Agency's (IAEA) simulation system, Nuclear Fuel Cycle Simulation System (NFCSS) was used to model fuel cycle components of the NES. NFCSS is a scenario based computer model for the estimation of nuclear fuel cycle material and service requirements. It has been designed to quickly estimate long-term fuel cycle requirements and actinide production. Natural uranium, conversion, enrichment, and fuel fabrication quantities are predicted. Additionally, the quantities and qualities (isotopic composition) of unloaded fuels are evaluated.

The numerical computing environment and programming language MATLAB® serves as the shell, or driver, for the simulated nuclear energy system by interfacing the configuration of nuclear reactors and corresponding fuel cycle components. Simulink®, an extension of MATLAB®, is utilized for storing system output results and parameters and tracking material streams throughout the NES. The UQ and optimization techniques are developed and implemented within the MATLAB® environment.

6 SYSTEM PARAMETERIZATION AND REPRESENTATIVE MODELS

The NES is composed of different reactors and components that work in coordination with each other to produce the desired output. Each has its own function and can be described in a stand alone fashion. This chapter describes each of the reactor units and fuel cycle components along with the models created to represent each. When possible experiment-to-code and code-to-code benchmarking procedures were applied and the results are presented within.

6.1 Reactor Units

The performance of the NES is heavily based on the reactor units. The three reactors selected for the system are the AP1000, VHTR, and HEST. The AP1000 is a Gen-III+ PWR design by Westinghouse. The VHTR is a Gen-IV design and currently the candidate for the NGNP. It is the prismatic core design and utilizes the TRIstructual ISOtropic coated fuel particles (TRISO) fuel type. The HEST is a subcritical system that takes advantage of the high energy 14.1 MeV neutrons produced by the D-T fusion reaction to drive the system and eliminate waste.

6.1.1 AP1000

The AP1000 is a Westinghouse Electric Company reactor design and is the first Generation III+ reactor to receive final design approval from the NRC. The AP1000 is a two-loop PWR planned to produce 1154 MWe. The design is built on proven technology from over 35 years of PWR operating experience. Major improvements over Gen.III reactors include the utilization of passive safety technology, overall system simplification, and modular construction. Making the AP1000 safer, and also easier and less expensive to build, operate, and maintain.

In the near future the AP1000 is expected to play a large role in nuclear energy generation worldwide. As indication, the Sanmen Nuclear Power Plant in Zhejiang China began construction of two AP1000s in February 2008, which are scheduled for operation during 2013-15. Another two units started construction in July 2008 at the Haiyang Nuclear Power Plant in Shandong. China has officially adopted the AP1000 as a standard for inland nuclear projects. Additionally, in the US, twelve Combined Construction and Operating Licenses (COLs) have been submitted as of 2009. The AP1000 is seen as the new standard for nuclear energy generation and will bridge the gap from yesterday's Gen-III technology to the advanced Gen-IV reactor systems of the future.

The major design parameters for the AP1000 are similar to that of other PWRs. The thermal power is rated at 3415 MW_{th} and with a thermodynamic efficiency of 32.7% it can produce a usable electrical power of 1117 MW_e. The fuel type is enriched uranium dioxide and the coolant/moderator is light water. A list of the AP1000 design parameters are provided in Table 6.1.

Table 6.1. AP1000 Design Parameters.

Parameter	Value
Thermal power (MW_{th})	3400
Electrical power (MW_e)	1115
Thermodynamic efficiency (%)	32.8
Fuel	UO_2
Average fuel enrichment (wt %)	4.8
Type of fuel assembly	17x17
Number of fuel assemblies	157
Active fuel length (m)	4.3
Equivalent core diameter (m)	3.04
Operating cycle length (months)	18
Linear heat rating (kW/m)	18.7
Operating pressure	15.5 Mpa
Coolant	light water
Coolant inlet temperature (°C)	280.7
Coolant outlet temperature (°C)	321.1

6.1.2 Model Description

The model is based on the AP1000 Design Control Documentation [22] provided by the US NRC. The reactor core consists of 157 fuel assemblies that are arranged in a pattern which approximates a right circular cylinder. Each fuel assembly contains 264 fuel rods, 24 guide tubes for control rod clusters, and 1 centrally located guide tube for in-core instrumentation, all of which are arranged in a 17 x 17 square lattice array. Figure 6.1 shows a cross-sectional view of the fuel assembly and related fuel rod and guide tube placements.

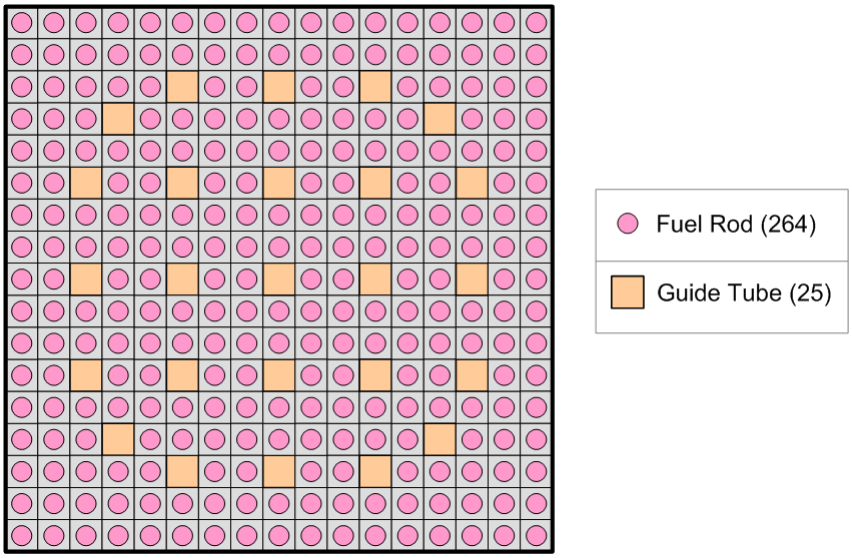

Figure 6.1. Fuel Assembly.

The model design is based on the initial core loading, in which the fuel rods within any given assembly have the same uranium enrichment in both the radial and axial planes. Fuel assemblies of three different enrichments are used to establish a favorable radial power distribution. Figure 6.2 shows the fuel assembly loading pattern used for the AP1000 model. It also shows the placement of the assemblies containing the Discrete Burnable Absorber Rods (PYREX) and Integral Fuel Burnable Absorber (IFBA) rods within the core.

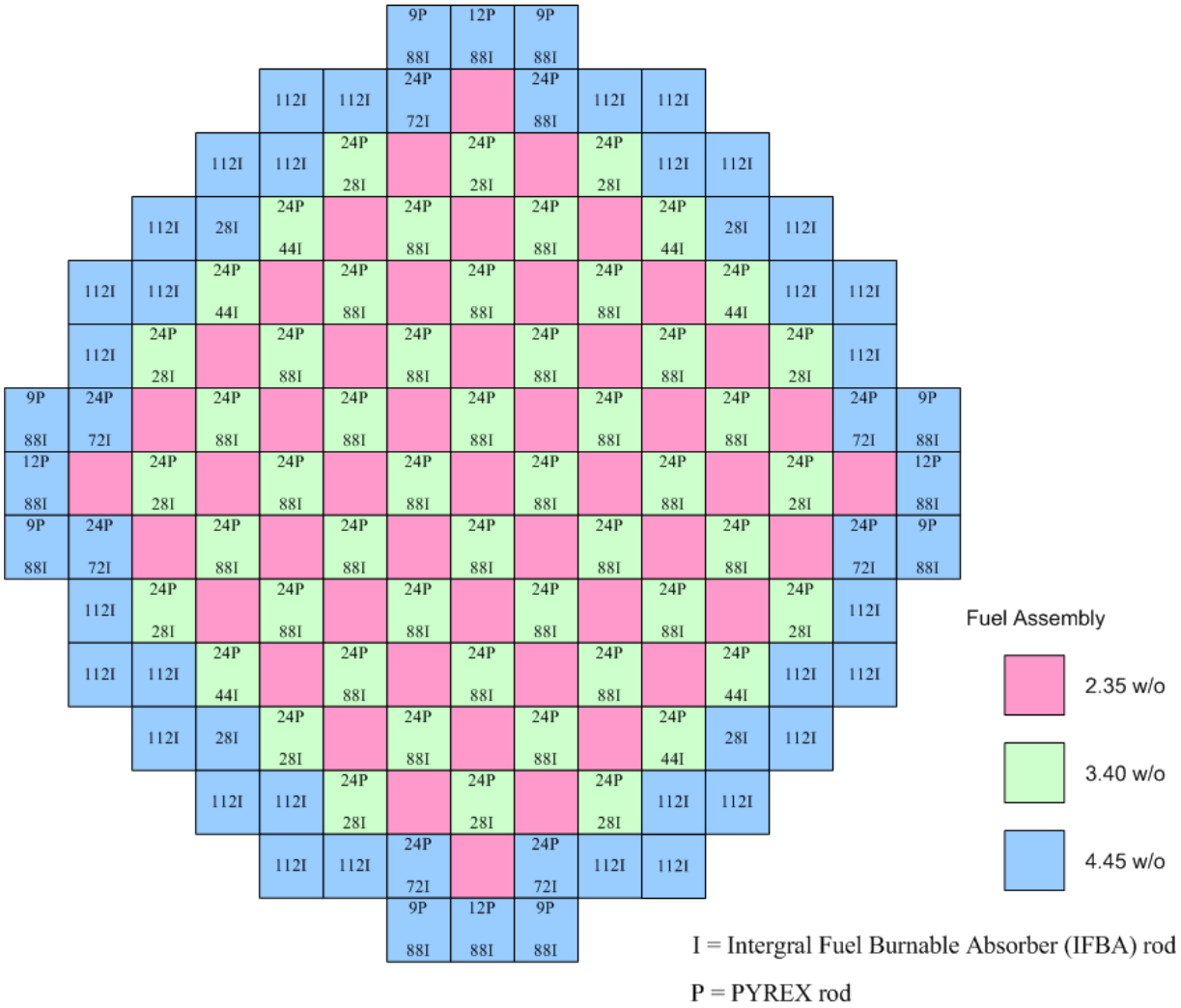

Figure 6.2. AP1000 Reactor Core Map.

Burnable absorbers in the form of PYREX and IFBA rods are used to provide partial control of the excess reactivity present during the fuel cycle. Their main function is to limit peaking factors and prevent the moderator temperature coefficient from being positive at normal operating conditions. Within a chosen fuel assembly the PYREX rods can be arranged in one of three different configurations, as shown in Figure 6.3. Similarly, the IFBA rods can be arranged in five different configurations and are shown in Figure 6.4. The placement of the assemblies

containing the burnable absorber within the core is displayed in Figure 6.2. A description of the reactor core, including dimensions and core materials is provided in Table 6.2.

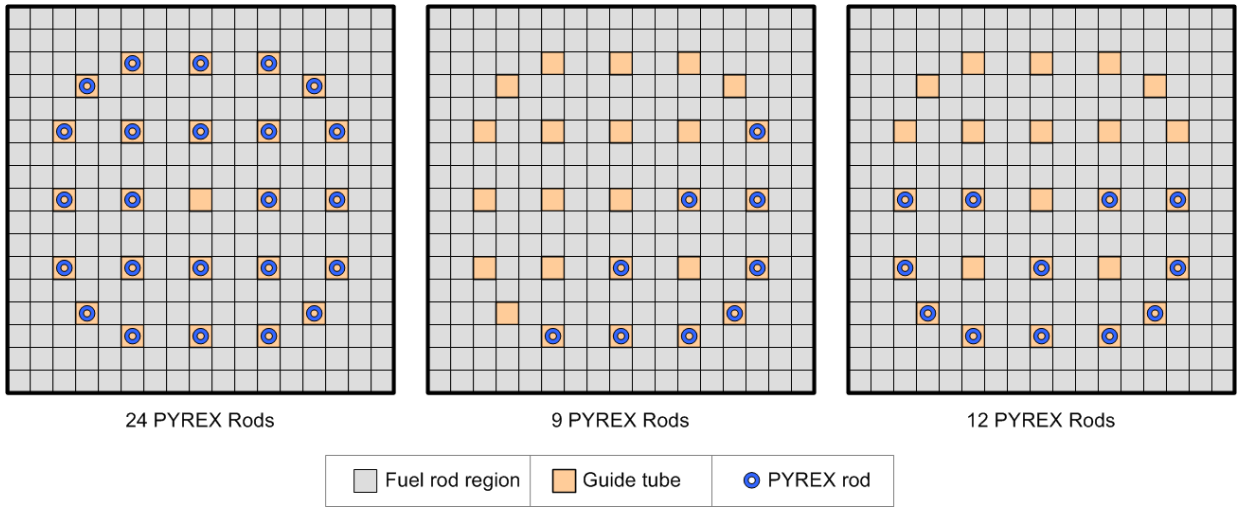

Figure 6.3. PYREX Rod Arrangement within the Fuel Assembly.

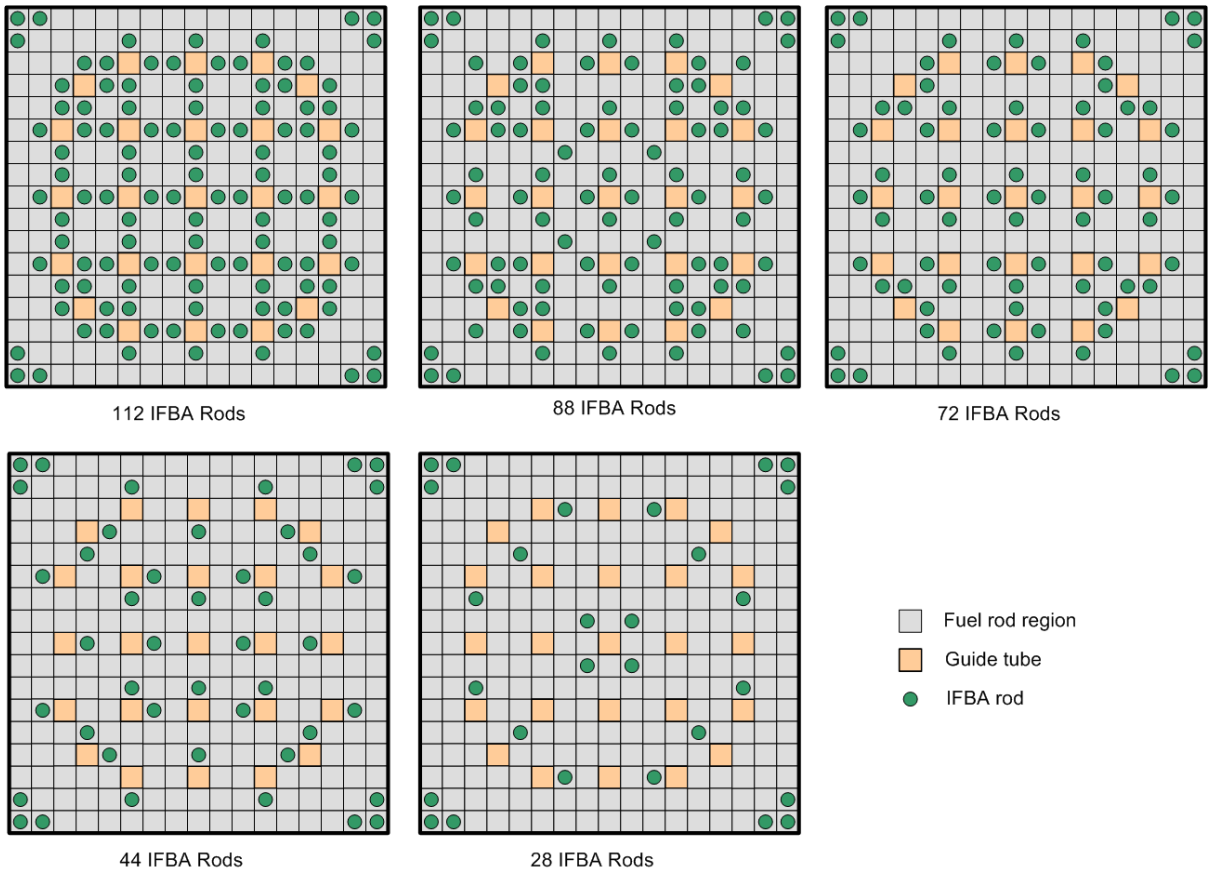

Figure 6.4. IFBA Rod Arrangement within the Fuel Assembly.

Table 6.2. Reactor Core Description.

Actice Core	
Equivalent diameter (cm)	304.04
Active fuel height (cm)	426.72
Height-to-diamter ration	78.14
Total cross section area (m²)	7.26
Fuel weight, as UO2 (g)	9.76E+07
Fuel Assembly	
Number	157
Rod array	17x17
Rods per assembly	264
Rod pitch (cm)	1.26
Overall transverse dimensions (cm)	21.40
Fuel Rods	
Number	41448
Outside diameter (cm)	0.9500
Gap diameter (cm)	0.0165
Clad thickness (cm)	0.0572
Clad material	ZIRLO
Fuel Pellets	
Material	UO2 sintered
Density (% theoretical)	95.5
Fuel Enrichments (weigth percent)	
Region 1	2.35
Region 2	3.40
Region 3	4.45
Diameter (cm)	0.819
Length (cm)	0.983
Discrete Burnable Absorber Rods (PYREX)	
Number	1558
Material	Borosilicate Glass
Outside diameter (cm)	0.968
Inner diameter (cm)	0.461
Clad material	Stainless Steel
B10 content (Mg/cm)	6.24
Absorber length (cm)	368.30
Integral Fuel Burnable Absorbers (IFBA)	
Number	8832
Type	IFBA
Material	Boride Coating
B10 content (Mg/cm)	0.772
Absorber lenth (cm)	386.08
Absorber coating thickness (cm)	0.00256

6.1.3 Benchmark Analysis

To test the validity of the AP1000 whole-core 3D model a benchmark test was developed. The AP1000 Design Control Documentation [22] provided by the US NRC for the licensing process was used for the procedure. The report provided the multiplication factor (k-eff) for cold, zero power, beginning of cycle, zero soluble boron core conditions. The code systems, MCNP5/MCNPX and SCALE 5.1 were used to model the reactor at the specified core conditions in order to benchmark the k-eff value against the published value and for a code-to-code benchmark procedure.

For both the MCNP and SCALE calculations the solution was obtained using one-million neutron histories, 5,000 histories per cycle for 260 cycles with the first 60 cycles ignored. The results are listed in Table 6.3. As indicated, the MCNP calculation was very accurate when compared to the published results, giving a difference of only 0.0498% between k-eff values. The result calculated by SCALE had a slightly higher difference at 0.1942%, and when comparing the two codes systems (MCNP vs. SCALE) the difference was measured at 0.1445%.

Table 6.3. Multiplication Factor Results.

Multiplication Factor Origin	k-eff	% difference (published-to-code)	% difference (code-to-code)
AP1000 Design Control Document	1.205	na	na
MCNP Code System	1.20440 ± 0.00062	0.0498	0.1445
SCALE Code System	1.20266 ± 0.00073	0.1942	

The average energy-dependent neutron flux in the fuel elements, as produced by MCNP and SCALE are provided in Figure 6.5. As shown, the profile is as expected for a PWR, but what is of more interest is the direct comparison of the two code systems. It is easily determined that spectrum produced by MCNP and SCALE are nearly identical, as they appear to be directly on top of each other.

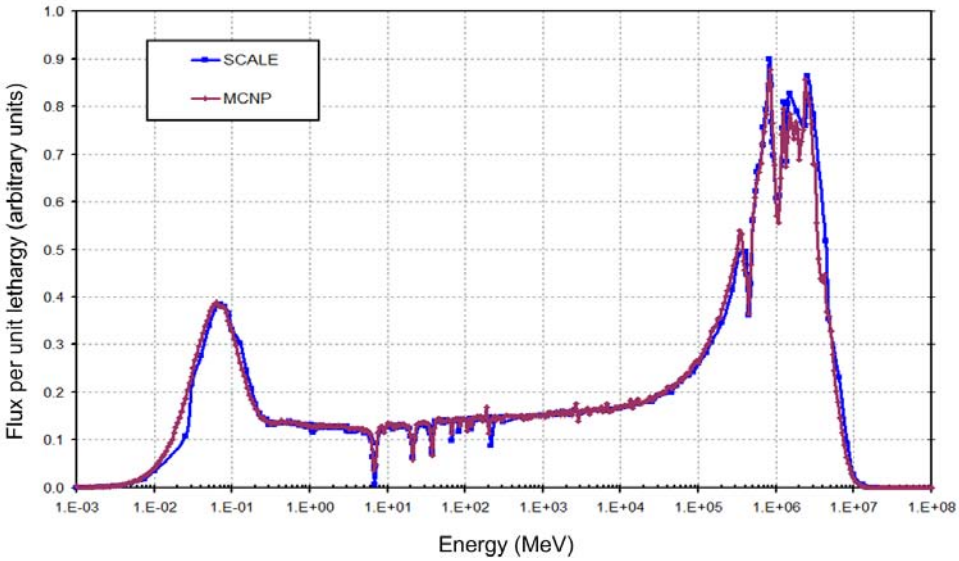

Figure 6.5. Neutron Flux Profiles in the Fuel Rods (MCNP vs. SCALE).

6.1.4 VHTR

DOE has given priority to the VHTR concept making it the focus of intensive research programs. The VHTR is designed to be a high-efficiency system, which can supply electricity and process heat to a wide-range of high temperature and energy intensive applications. The VHTR is a passively safe design. The refractory core, low power density, and low excess reactivity enable this design feature.

The VHTR is a graphite moderated gas-cooled reactor that supplies heat with core outlet temperatures in the range of 850 - 1000 degree Celsius, which enables applications such as hydrogen production, process heat for the petrochemical industry, or sea water desalination. Its basic technology has been well established in former High Temperature Gas Reactors (HTGR), such as the German AVR and THTR prototypes, and the US Fort Saint Vrain and Peach Bottom prototypes. The VHTR extends the capabilities of HTGR's to achieve further improvements in thermal efficiency and open up additional high-temperature applications.

The reactor core can be a prismatic block core or a pebble bed core design. Both the prismatic and pebble bed cores have the same key design characteristics and use the same ceramic or TRISO (TRIstructual ISOtropic) coated fuel particles. The TRISO coating provides a miniature containment vessel for each fuel particle, allowing complete retention of fission fragments at high temperatures [23].

The core type utilized in the nuclear energy system is the prismatic block design. The prototypical prismatic VHTR produces a thermal power of 600 MW_{th} with a low power density of approximately 7 W/cm³ and an annular fuel configuration. In basic terms, the core is composed of fuel blocks, control rod guide blocks, and reflectors blocks. The fuel blocks consist of a hexagonal graphite block with borings for the placement of fuel compacts and helium

coolant channels. The control rod guide blocks are hexagonal graphite blocks with borings for the control rods to pass through. The reflector blocks are simply solid graphite hexagonal blocks used to limit neutron leakage. The fuel blocks, control rod guide blocks, and reflector blocks are stacked on top of one another and then arranged side-to-side in a hexagonal lattice to create a cylindrically shaped core.

6.1.5 Model Description

The VHTR model is based on the High Temperature Test Reactor (HTTR) of the Japan Atomic Energy Research Institute (JAERI) [24]. The HTTR was selected because of the provided experimental test results and the opportunity it presented for performing an experiment-to-code benchmark analysis, as detailed later in this section. The basic design features of the smaller HTTR were used to create the scaled-up VHTR power reactor. The VHTR design parameters are listed in Table 6.4.

Table 6.4. VHTR Design Parameters.

Fuel	UO_2	Power (MW_{th})	*600*
Enrichment(%)	*8*	Power Density (W/cm³)	*6.9*
Coolant	*He*	Pressure (MPa)	*7.0*
		Inlet/Outlet Temperature (°C)	*490/950*
# of Columns	*102*	# of Fuel Columns	*66*
		# of Control Columns	*36*
		# of Blocks/Column	*13*
Block Pitch (cm)	*36*	# of Fuel Pins/Fuel Block	*32*
Block Height (cm)	*58*	# of Burnable Posion Rods/Fuel Block	*2*
		Control Rods/Control Block	*2*
		Emergency Rods/Control Block	*1*
		Compact Pitch (cm)	*5.15*
		Fuel Hole Radius (cm)	*4.1*
		Compact Inner Radius (cm)	*0.5*
		Compact Outer Radius (cm)	*1.3*
Packing (%)	*30*	10.41 g/cm³ Kernel Radius (cm)	*0.0300*
		1.14 g/cm³ Buffer Radius (cm)	*0.0359*
		1.89 g/cm³ PyC1 Radius (cm)	*0.0390*
		3.20 g/cm³ SiC Radius (cm)	*0.0419*
		1.87 g/cm³ PyC2 Radius (cm)	*0.0465*
		Matrix (g/cm³)	*1.77*
		Block (g/cm³)	*1.69*

The general procedure for creating the model was to build the three types of prismatic hexagonal blocks that compose the VHTR, and then arrange these blocks in an array of rows and columns to construct the core. The three prismatic blocks include: fuel assembly blocks, replaceable

reflector blocks, and control rod guide blocks. The configuration of prismatic blocks was then surrounded by a permanent graphite reflector to complete the core.

The fuel assemble block consists of 33 fuel elements with helium coolant channels and two burnable poison rods, which are arranged in a hexagonal graphite block to create a pin-in-block type assembly. The fuel block is 36 cm in width across the flats and 58 cm in height. The block has 33 vertical borings with a diameter of 4.1 cm for placement of the annular fuel rods. In addition, each fuel graphite block has three burnable poison insertion holes measuring 50 cm in height and 1.5 cm in diameter. Two are loaded with burnable poison rods, while the third is left empty. In the center of each block is a fuel handling hole. Figure 6.6 shows the arrangement and dimensions of the prismatic fuel block. The measurements and material properties of the block are given in Table 6.5.

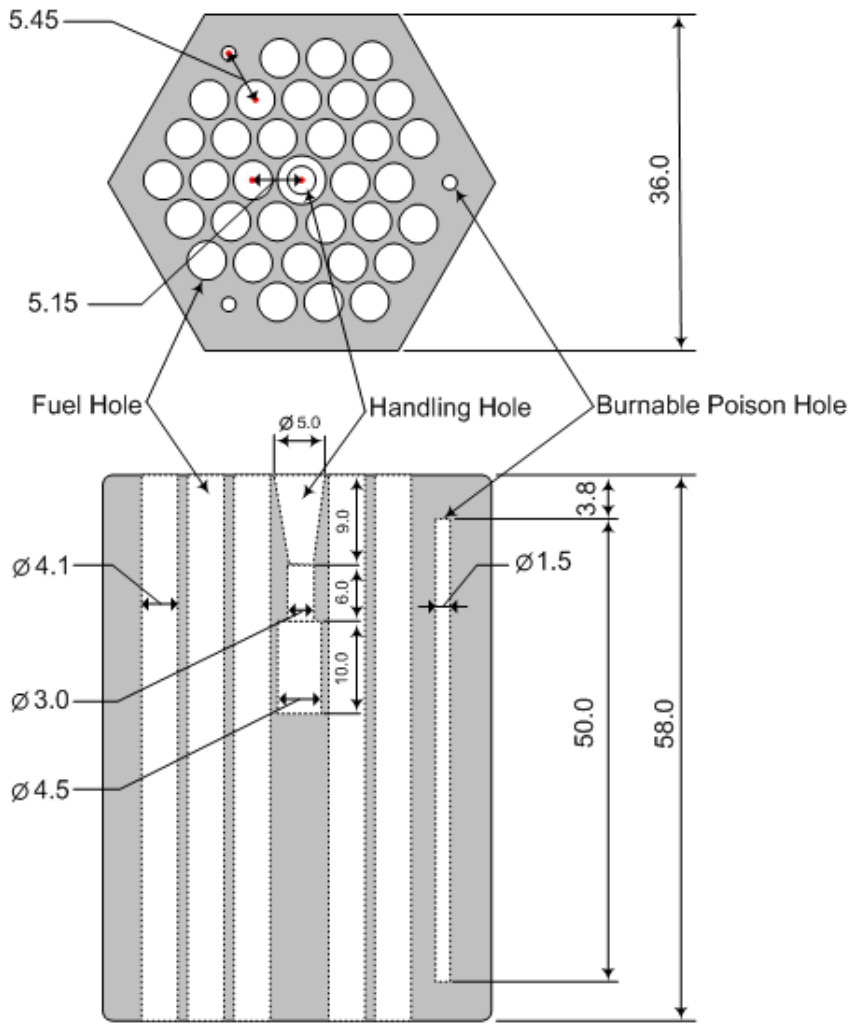

Figure 6.6. Prismatic Fuel Block (measurements in cm).

Table 6.5. Prismatic Fuel Block Properties.

Type	Pin-in-block
Configuration	Hexagonal
Material	IG-110 Graphite
Density (g/cm³)	1.77
Height (cm)	58
Width Across the Flats (cm)	36
# of Fuel Holes/Block	33
Fuel Hole Diameter (cm)	4.1
Fuel Hole Height (cm)	58
# of Burnable Poison Holes/Block	3
Burnable Poison Hole Diameter (cm)	1.5
Burnable Poison Hole Height (cm)	50

The fuel element consists of TRISO fuel particles imbedded within a graphite matrix in the form an annular rod (fuel compact) which is encapsulated by a graphite sleeve. Figure 6.7 illustrates how the TRISO particles, fuel compact, and protective sleeve are arranged to create the fuel element. Each fuel element contains 176,515 TRISO particles within the fuel compact with a packing fraction of 30%. Table 6.6 contains the fuel element dimensions and material properties. The MCNP model uses a square lattice array for the TRISO particles contained in the graphite matrix of the fuel compact.

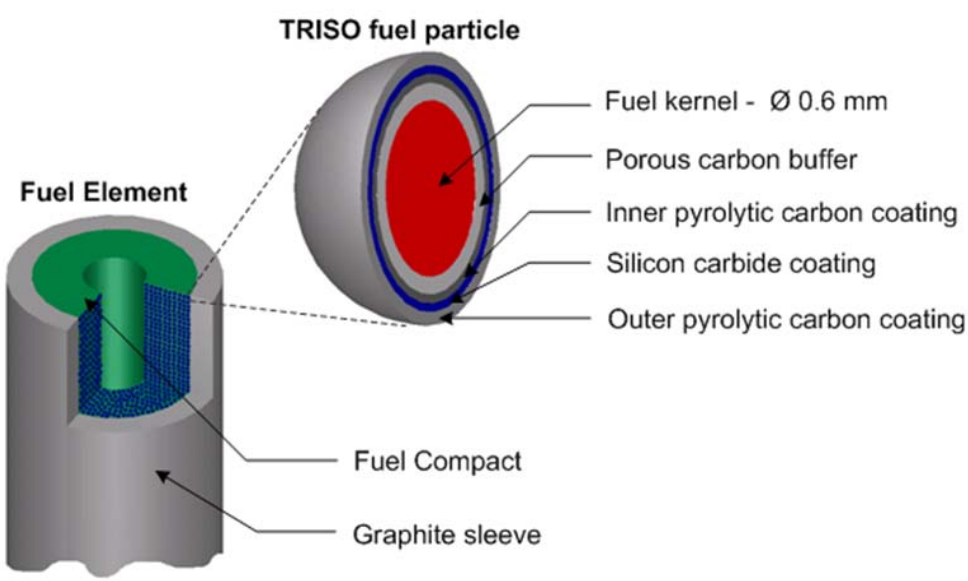

Figure 6.7. VHTR Fuel Element.

Table 6.6. Fuel Element Properties.

a) TRISO particle	Material	Density (g/cm³)	Radius (cm)
Fuel kernel	UO_2	10.41	0.0300
1st costing	PyC	1.14	0.0359
2nd coating	PyC	1.89	0.0390
3rd coating	SiC	3.2	0.0419
4th coating	PyC	1.87	0.0465

b) Fuel Compact	
Number of fuel particles	176,515
Graphite matrix density	1.690 g/cm³
Diameter-inner	1.0 cm
Diameter-outer	2.6 cm
Height	54.6 cm

c) Graphite Sleeve	
Material	Graphite
Density	1.770 g/cm³
Diameter-inner	2.6 cm
Diameter-outer	3.4 cm
Height	57.7 cm

The burnable poison rod is 1.4 cm in diameter and 50 cm in height. It is made up of two neutron absorber sections (20 cm in height) separated by a graphite section (10 cm in height). Table 6.7 lists the properties of the burnable poison rods.

Figure 6.8 shows a three-dimensional representation of the prismatic fuel block and the relative locations of the annular fuel rods, coolant channels, burnable poison rods, and fuel handling hole. Within the core there are 858 fuel blocks.

Table 6.7. Burnable Poison Rod Properties.

Absorber Section Material	B_4C-C
Density (g/cm³)	*1.82*
Natural Boron Concentration (wt. %)	*2.74*
Diameter (cm)	*1.39*
Height (cm)	*2.5*
B-10 Abundance Ratio (wt. %)	*18.7*
Graphite Section Density (g/cm³)	*1.77*
Diameter (cm)	*1.4*
Height (cm)	*10*

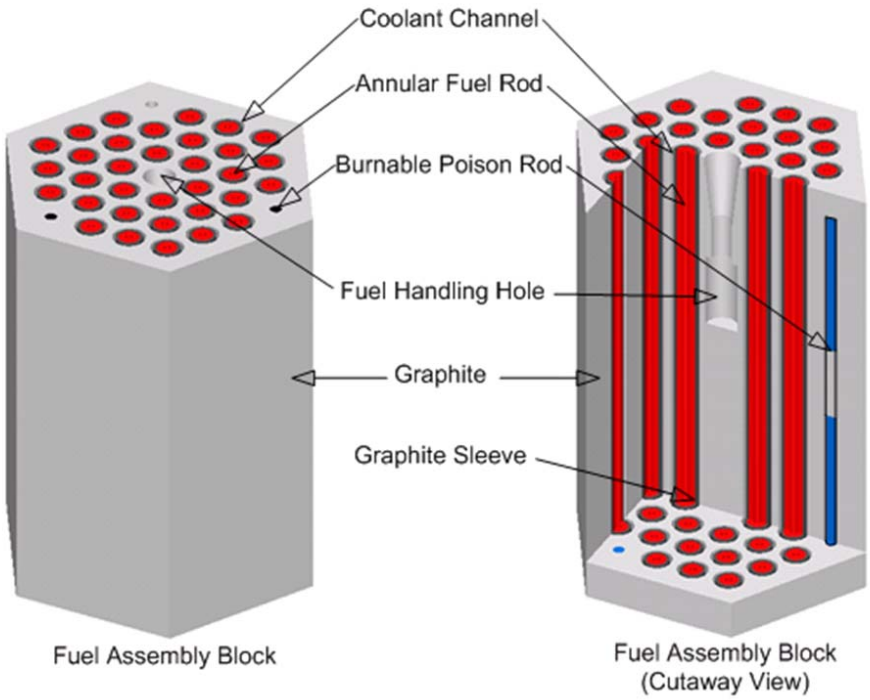

Figure 6.8. VHTR Prismatic Fuel Block.

The replaceable reflector block has the same external form as the fuel assembly block, 36 cm in width across the flats and 58 cm in height with a handling hole in the center of the block. There are two types of reflector blocks; one being a solid graphite block, and the other having helium coolant channels in it. Examples of the replaceable reflector blocks are provided in Figure 6.9, with the properties listed in Table 6.8.

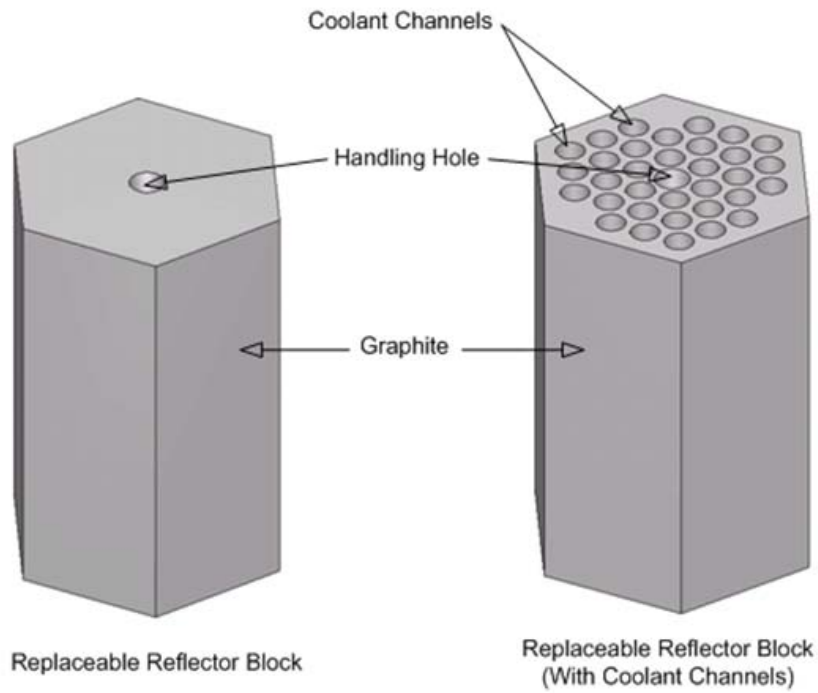

Figure 6.9. Replaceable Reflector Blocks.

Table 6.8 Replaceable Reflector Block Properties.

Configuration	*Hexagonal*
Material	*IG-110 Graphite*
Density (g/cm³)	*1.76*
Height (cm)	*58*
Width across the flats (cm)	*36*
Coolant hole diameter (cm)	*4.1*
Coolant hole height (cm)	*58*

The reflector blocks with the coolant channels are stacked directly above and below the fuel assembly blocks. This creates a fuel column, being composed of 2 replaceable reflector blocks on top, 13 fuel assembly blocks in the middle (active core), and 2 replaceable reflector blocks on the bottom. The replaceable reflector blocks with coolant channels have the same dimensions as the fuel graphite block within the same column, with the exception of not having the three burnable poison insertion holes. This allows the helium gas coolant to flow into the core, through the fuel assemble blocks and around the fuel elements, and then exit the core.

The final type of prismatic block is the control rod guide block. The block consists of a hexagonal graphite block with three large vertical borings. Just as the fuel block, it is 58 cm in height and 36 cm in width across the flats. The holes created by the borings have a 12.3 cm diameter and extend through the entire length of the block. Two of the holes are used for the

control rods to pass through, while the third is left empty to serve as the reserve shutdown system. In the center of each block is a fuel handling hole. Figure 6.10 shows the arrangement and dimensions of the fuel graphite block and Table 6.9 lists the properties of the block.

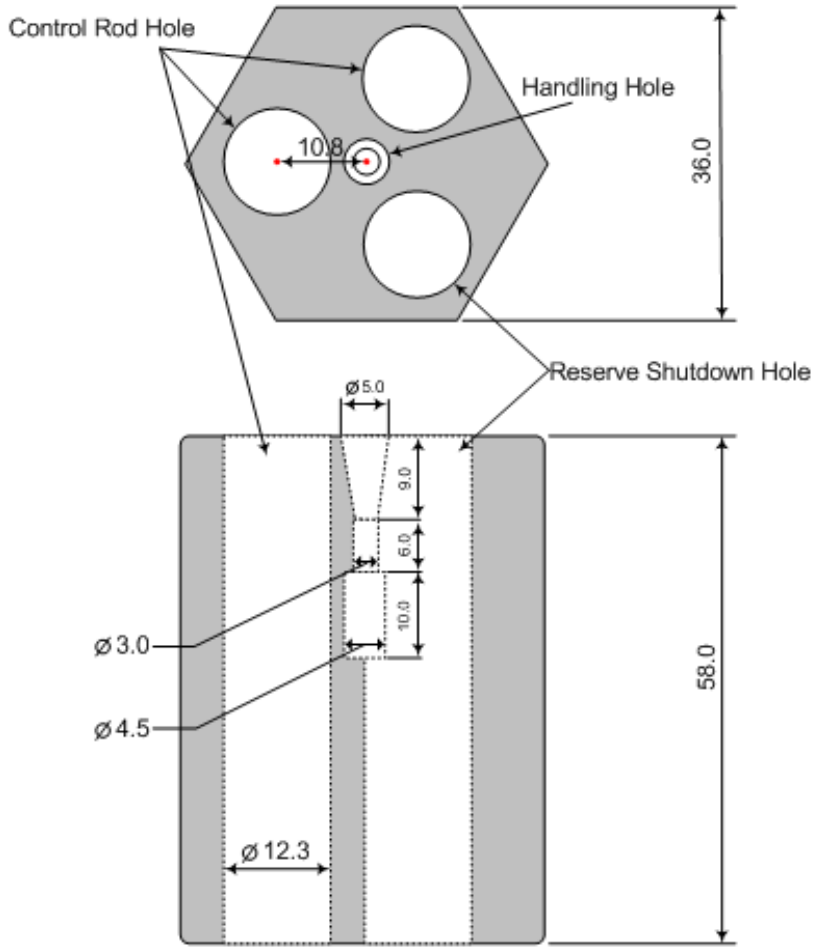

Figure 6.10. Control Rod Guide Block (measurements in cm).

Table 6.9 Control Rod Guide Block Properties.

Material	*IG-110 Graphite*
Density (g/cm³)	*1.77*
Height (cm)	*58*
Width across the flats (cm)	*36*
Number of control rod holes in block	*2*
Control rod hole diameter (cm)	*12.3*
Control rod hole height (cm)	*58*
Number of reserve shutdown holes in block	*1*
Reserve shutdown hole diameter (cm)	*12.3*
Reserve shutdown hole height (cm)	*58*

The model can now be described by fuel columns, control columns, the central reflector, and the outer reflector. The fuel and control columns are arranged in an annular configuration that is three blocks wide to create the fueled region of the core. The central graphite column and surrounding graphite reflector make up the remainder of the core. The active core is composed of 66 fuel columns and 36 control columns that have 13 blocks per column. The bottom reflector is 160 cm thick and the top reflector is 116 cm thick. The active core is 754 cm in height and the overall core is 1030 cm in height. The radial distance from the center of the core to the closest fuel column is 144 cm and the fueled region is 108 cm thick (three fuel/control columns across). The outer reflector is 88 cm thick giving an outer cylindrical core radius of 340 cm. Figure 6.11 shows a 3D and 2D view of the VHTR model with geometry details.

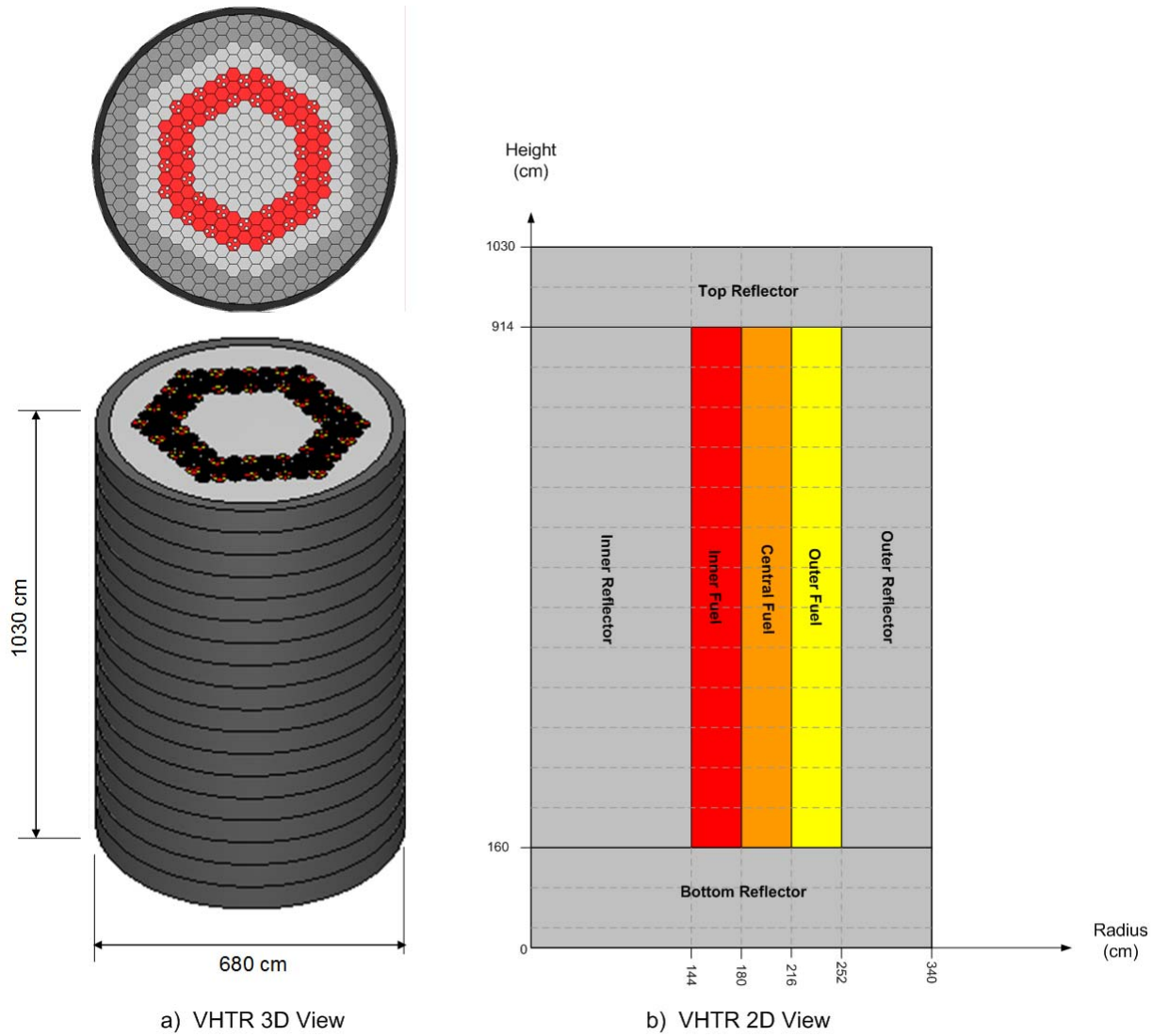

Figure 6.11. VHTR Whole-Core 3D Model Geometry Details.

6.1.6 Benchmark Analysis

Many of the well established computer code systems available for VHTR analysis were originally developed and validated for the purpose of evaluating Light Water Reactor (LWRs). Although VHTRs and LWRs are both thermal reactors and share much in common, the VHTR presents unique phenomena that may not be accounted for correctly by the code system and therefore must be addressed. Of main concern is the randomness in particle distribution and related multi-heterogeneity effects associated with VHTRs. Due to this concern a detailed benchmark procedure was developed for the VHTR model.

High importance was placed on the ability to perform experiment-to-code benchmarking and to combine that with additional code-to-code comparisons. The availability of experimental results led to the HTTR of the JAERI, from which startup core physics results are provided by the IAEA in a Technical Document publication [24]. The major design specifications for the HTTR are given in Table 6.10.

Table 6.10. HTTR Design Specifications.

Thermal Power (MW)	*30*
Outlet Coolant Temperature (°C)	*950*
Inlet Coolant Temperature (°C)	*395*
Primary Coolant Pressure (MPa)	*4*
Core Structure	*Graphite*
Equivalent Core Diameter (cm)	*230*
Effective Core Height (cm)	*290*
Average Power Density (W/cm³)	*2.5*
Fuel	*UO_2*
Uranium Enrichment (wt. %)	*3 to 10*
Type of Fuel	*Pin-in-block*
Burnup Period (days)	*660*
Coolant Material	*Helium gas*
Flow Direction in Core	*Downward*
Top Reflector Thickness (cm)	*116*
Side Reflector Thickness (cm)	*99*
Bottom Reflector Thickness (cm)	*116*
Number of Fuel Assemblies	*150*
Number of Fuel Columns	*30*
Number of Pairs of Control Rods	*16*
In Core	*7*
In Reflector	*9*

In addition to the HTTR benchmark model description provided in this section, complete details of material compositions and geometry specifications are included in Appendix A. The SCALE code system was chosen as the computational tool for modeling the HTTR due to its flexibility in geometry representation, existing temperature treatment options, availability of techniques accounting for double heterogeneity effects, and computational run time for complex whole-core 3D models.

An assessment was performed to determine the best method for accounting for the double heterogeneity effects, as detailed by Ames [25]. This was accomplished by creating two HTTR models, one using the provided DOUBLEHET unit cell treatment available in SCALE 5.1, while the other bypasses the feature and instead the Dancoff correction factor is independently determined by the code system DANCOFF-MC [26] and manually entered into the model as an external parameter. Table 6.11 provides a comparison of the results for the two different treatments accounting for the heterogeneity effects. As shown, a higher degree of accuracy was accomplished with the DOUBLEHET model, therefore it was chosen to represent the HTTR model for further benchmark efforts.

Table 6.11. Results for Different Heterogeneity Treatments.

HTTR Model	k-eff	Error (%)
Experimental	*1.1363*	-
SCALE 5.0 (with DANCOFF-MC)	*1.1122*	*2.12%*
SCALE 5.1 (with DOUBLEHET)	*1.1368*	*0.04%*

The benchmark problems are related to start-up core physics tests and include the analysis of the effective multiplication factor for the fully loaded core with control rods fully withdrawn and fully inserted, control rod position at criticality, and the isothermal temperature coefficient of reactivity.

Following the established international benchmark program practices, in the present analysis 10% discrepancy between computed values and the available experimental values was considered as the model acceptability threshold. As evident in Table 6.12 the results are well within the acceptable range. Aside from the temperature coefficient, each of the benchmark cases is within 0.25% of the experimental values and fall within the experimental error value. The computed value of the isothermal temperature coefficient deviates by about 2% from the corresponding experimental value. However, the experimental value is within the standard deviation limits of the computational result. It is expected that increasing the sample size of the model would result in reducing the discrepancy to within the range of the other benchmark tests, but for the benchmark calculations a maximum computational run time was set and higher accuracy results were not obtained in the present analysis.

Table 6.12. Experiment-to-Code Benchmark Results.

Benchmark		HTTR (experimental)	VHTR model (calculated)	Error (%)
Control Rods Fully Withdrawn	k-eff	1.1363 ± 0.041	*1.1368 ± 0.0023*	*0.044*
Control Rods Fully Inserted	k-eff	0.685 ± 0.010	*0.6858 ± 0.0019*	*0.117*
Critical Insertion Depth (300K)	cm	177.5 ± 0.5	*177.1*	*0.225*
Critical Insertion Depth (418K)	cm	190.3 ± 0.5	*189.9*	*0.210*
Temperature Coefficient	dk/k/K	-1.42E-04	*-1.45E-04*	*2.113*

The HTTR configuration with the control rods fully withdrawn was chosen as the prototype VHTR configuration. The best agreement with experimental data was observed for that case. Table 6.13 summarizes the basic reactor physics characteristics obtained for the prototype VHTR configuration.

Table 6.13. Basic Reactor Physics (Withdrawn Control Rods).

k-eff	Fission-Inducing Energy (eV)	System Mean Free Path (cm)	Fission Neutorn Yield
1.1368 ± 0.0023	*0.814041 ± 0.0002014*	*2.9445 ± 0.00121*	*2.43872 ± 0.00001*

The HTTR is currently the only operating VHTR prismatic core design, making it a focal point for VHTR related research. The HTTR was designed according to established objectives, which categorize it as a small-scale VHTR. The future VHTR power reactors will most likely consist of annular core designs, whereas the HTTR is a cylindrical core design. An annular core is one of the promising core types for the future VHTRs because of its high inherent safety characteristics following a loss of coolant accident. The decay heat removal is enhanced by the introduction of the annular core because the heat transfer path will be shortened due to the relatively thin active core region. As a result, the fuel temperature in a loss of coolant accident can be maintained at less than the fuel temperature limit of 1600 °C [27].

The prismatic whole-core 3D model was adjusted from the original cylindrical core of the HTTR to that of a larger annular power core (600 MW_{th}), which represents the VHTR model used in the nuclear energy system within this study and is described by Table 6.4 and Figure 6.11.

To maintain the consistency of the annular VHTR model an exact model was built in MCNP to perform a code-to-code benchmark for the new configuration. A comparison of the multiplication factor for the SCALE and MCNP models is provided in Table 6.14.

Table 6.14. Code-to-Code Results.

Code System	k-eff	% difference
MCNP	*1.26737*	*0.124*
SCALE	*1.26580*	

In addition to the multiplication factor the average energy-dependent neutron flux within the fuel compacts was also evaluated for the models. As shown in Figure 6.12 the flux profile is typical for that of VHTRs, but what is of more interest is the direct comparison of the spectrums produced by the two code systems, which are almost indistinguishable.

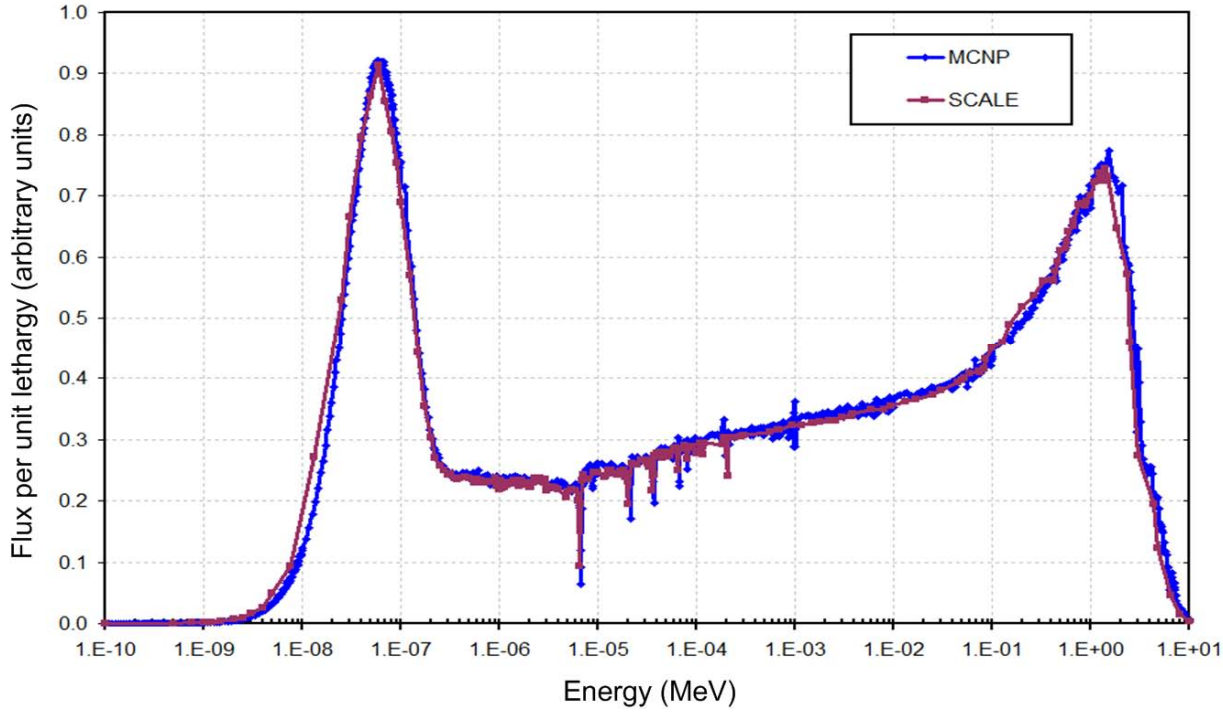

Figure 6.12. Neutron Flux Profiles in the Fuel Rods (MCNP vs. SCALE).

6.1.7 High-Energy External Source Transmuter

Subcritical cores driven by an external neutron source (often referred to as hybrid nuclear reactor systems) have been the subject of many research studies dating back to as early as the 1950s [28-30]. The foreseen advantages for fuel generation, energy production, and most recently waste minimization have driven such efforts. Even so, hybrid nuclear systems have never advanced past the conceptual study phase, making them quite different from the AP1000 and VHTR reactor units, which both (especially the AP1000) rely on previous operating experience and build on already proven designs.

In recent years a great deal of interest, or a renewal of interest, has been displayed worldwide in hybrid reactors mainly due to the perceived advantages for transmuting the long-lived actinides of spent nuclear fuel into a much more manageable waste form [8-14, 31]. These advantages stem from the safety features that accompany subcritical systems, allowing for extremely high transmutation efficiencies as compared to other options.

6.1.8 External Neutron Source Survey

Potential neutron sources for hybrid systems must meet two important criteria: 1) be a high intensity source and 2) produce high energy neutrons. In addition, the size of the neutron source can play an important role, with the ultimate goal being a small compact source.

Intense high energy neutron sources for hybrid systems can be separated into two general categories: 1) Accelerator Driven Systems (ADS) neutron sources, and 2) fusion neutron sources.

ADS neutron sources most commonly use proton accelerators, which deliver continuous wave neutron beams with an energy around 1GeV. The accelerator is either the linac or cyclotron type. The protons are impinged upon a heavy element spallation target to produce source neutrons. Somewhat less common is using accelerators for producing high energy charged particle beams (other than proton beams) coupled with spallation targets for producing neutrons.

The most promising fusion neutron sources use the neutrons produced from the deuterium and tritium fusion reaction as the source. The nuclei of two isotopes of hydrogen, Deuterium (D) and Tritium (T) react to produce a helium nucleus (α) and a neutron (n). In each reaction 17.6 MeV of energy is liberated:

$$D + T \rightarrow n\left(14.1\ MeV\right) + \alpha\left(3.5\ MeV\right)$$

There are a number of different options for creating the conditions necessary for the D-T fusion reaction, which are classified as follows:

- Strong magnetic field concepts: Use magnetic confinement schemes for fuel plasma
  - Tokamaks (pulsed)
  - Stellarators (continuous)
  - Mirror machines (continuous)
- Inertial confinement devices: process where nuclear fusion reactions are initiated by heating and compressing a fuel target, typically in the form of a pellet that most often contains a mixture of deuterium and tritium (pulsed).
  - Laser-driven inertial confinement: uses laser light to compress and heat target.
  - Z-pinch: intermediate of magnetic and inertial confinement. A type of plasma confinement system that uses an electrical current in the plasma to generate a magnetic field that compresses it.
- Muon-catalyzed fusion (μCF): process allowing nuclear fusion to take place at temperatures significantly lower than the temperatures required for thermonuclear fusion. (cold fusion)

6.1.9 Model Description

As part of the year 1 study the HEST model is in preliminary form. It was primarily created to get a feel for the neutronic properties of such a system and to be used to build upon in year 2 of the project. The model is a single fuel assembly block from the VHTR core (matching the description provided in section 6.1.2) with a high energy neutron point source placed in the center, as depicted in Figure 6.13.

The model was created with MCNP and uses the source definition card to place a 14.1 MeV neutron source at the center of the prismatic block. The fuel is Low Enriched Uranium (LEU) and is being used as a reference case. As the project continues and the HEST model evolves the fuel will be replaced by the VHTR used fuel.

Currently the model is not setup for criticality and depletion calculations, but will be implemented in the future. The future model will also take into account the parameters of fuel form, blanket configuration, source intensity, and source placement.

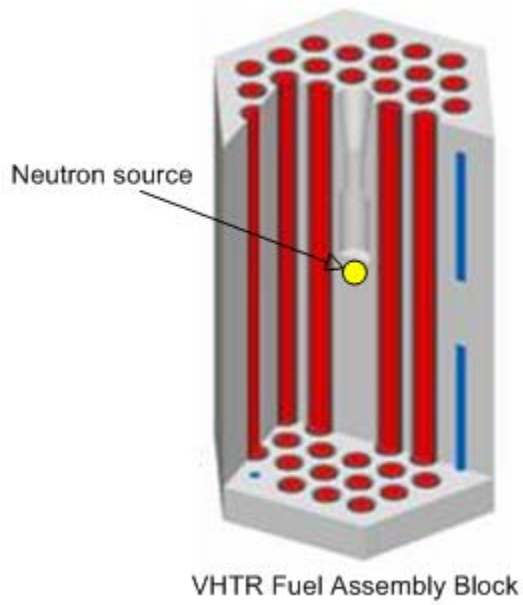

Figure 6.13. Prismatic Block with Neutron Source.

6.2 Fuel Cycle Components

6.2.1 Front-End Components

Accompanying the reactor units in NES are the fuel cycle components. Composing the front-end portion of the cycle are the mining, milling, conversion, enrichment, and fuel fabrication. As a result of front-end procedures DU and mill tailings are accumulated and must be stored as LLW. The main concern for the front-end is material flow and its effect on mining and waste storage strategies.

The IAEA's simulation system NFCSS was used to model the portion of the NES that includes the front-end components and the AP1000, as shown in Figure 6.14. NFCSS is a scenario based computer model for the estimation of nuclear fuel cycle material and service requirements. It has

been designed to quickly estimate long-term fuel cycle requirements and actinide production. Natural uranium, conversion, enrichment, and fuel fabrication quantities are predicted. Additionally, the quantities and qualities (isotopic composition) of unloaded fuels are evaluated.

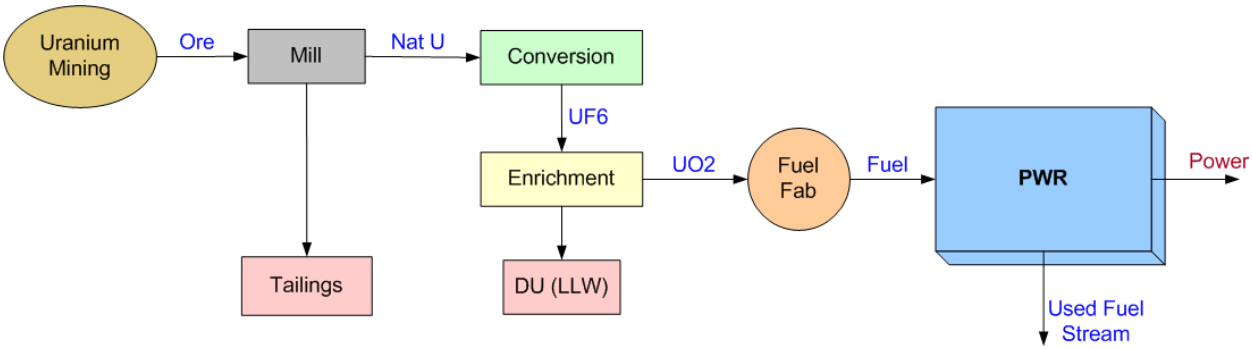

Figure 6.14. NFCSS Components.

The NFCSS model tracks the overall material flow in each of the processes described in the fuel cycle as presented in Figure 6.14. The model assumes zero losses in the conversion, enrichment, and fuel fabrication stages. The reactor model (fuel depletion model) is the most important part of the simulation since it calculates the inventory of used fuel after irradiation. The reactor model is required to be an optimum combination of simplicity, accuracy, and speed. Therefore the IAEA developed CAlculation of INventory of spent fuel (CAIN) specifically for the needs of NFCSS. CAIN solves the Bateman's Equations for a point assembly using one group neutron cross sections. In order to meet the accuracy, simplicity, and speed requirements a set of assumptions were built into the code. CAIN currently has 28 reaction and decay chains during irradiation and 14 decay chains during cooling. The main assumptions built into CAIN are listed as follows [32].

- The selection of the nuclides has been performed for the importance of the nuclides in radiotoxicity of the spent fuel and their nuclear characteristics.
- Although natural uranium includes U-234 (<0.01%), this nuclide is ignored, because the transmutation from U-234 to U-235 is too small.
- Nuclides with short half lives (half life < 8 days) are ignored. That is, U-237 (7 days), Np-238 (2 days), Pu-238 (5hrs), Am-242 (16 hrs), Am-244 (10 hrs), and Am-244m (26 min) are assumed to decay and go to the next nuclide simultaneously.
- Long half life nuclides (half life > 400 years) are assumed as stable for the irradiation period. As example, Am-241 (432 yr) is treated as stable during irradiation. For decay (cooling) period after discharge, all nuclides are treated by their actual decay scheme.
- In the chain shown in Figure 6.15 transmutation is terminated for certain nuclides (shown as mark "x").
- The 28 reaction chains and 14 decay chains are selected to be suitable for fresh fuels containing any of the 14 nuclides of the CAIN library. Some reaction chains are neglected due to their contribution to the composition of the spent fuel. The nuclides included in the calculations are listed in Table 6.15.

- Among 14 nuclides, decays of Pu-238 (87.7 yr), Pu-241 (14.4 yr), Cm-242 (0.447 yr), and Cm-244 (18.1 yr) are considered during irradiation. Figure 6.15 shows the transmutation chain after specification for the CAIN code.

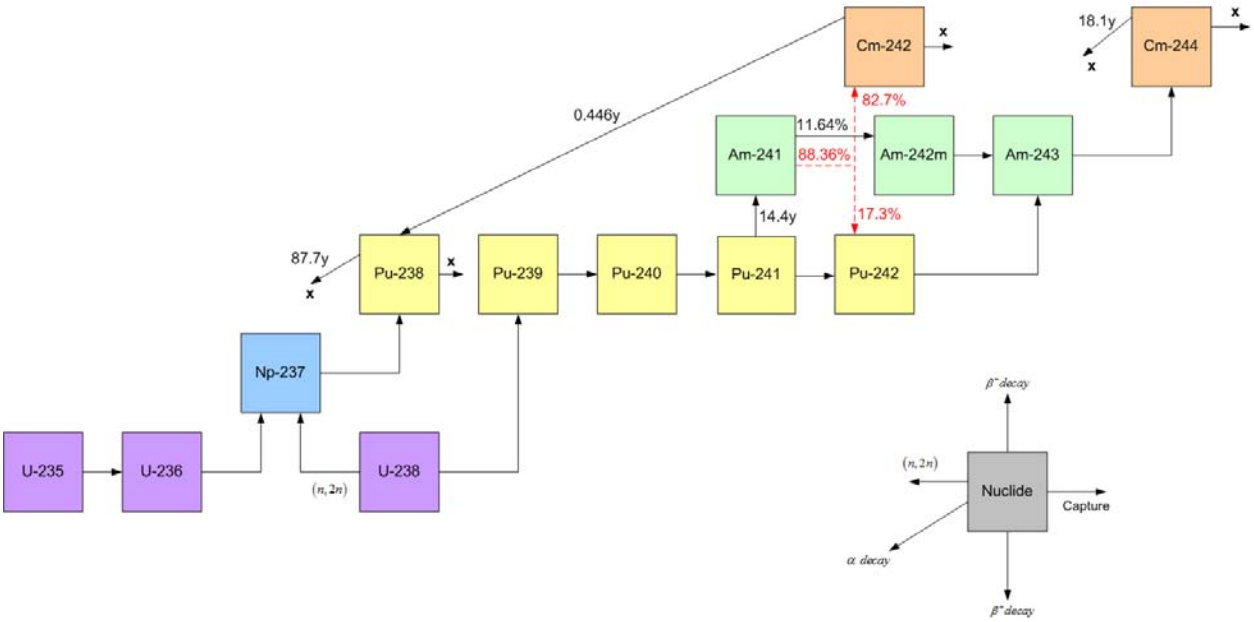

Figure 6.15. CAIN Transformation Chain.

Table 6.15 Nuclides Included in CAIN Calculation.

Uranium	U-235	U-236	U-238		
Neptunium	Np-237				
Plutonium	Pu-238	Pu-239	Pu-240	Pu-242	Pu-242
Americium	Am-241	Am-242m	Am-243		
Curium	Cm-242	Cm-244			

The input parameters for the model are mostly dependent on the parameters for the AP1000 model, with the exception of the grade of the uranium ore and the enrichment tail assay, which are both adjusted to current typical values for each case. The mine grade is set at a value of 1% uranium containment within the ore, and the tail assay, which is defined as the percent of U-235 remaining in the depleted stream of enrichment operations is 0.30%. The parameters consisting of reactor type, fuel type, power, and thermal efficiency are determined by the design parameters for the AP1000. The remaining input parameters of load factor, enrichment, and average discharge burnup are dependent on the optimum values determined for the NES. Table 6.16 lists the input parameters for the NFCSS.

The NFCSS model produces output indicating the required quantity of uranium ore, the natural uranium needed for the conversion process, amount of UF6 needed for enrichment, the final

quantity of UO2 for reactor operation, and amount of DU produced. The Separative Work Unit (SWU) is also calculated for the system along with the isotopic composition of the used fuel.

Table 6.16. NFCSS Input Parameters.

Reactor Type	PWR
Fuel Type	UO_2
Nuclear Power (MWe)	1115
Load Factor	Variable
Thermal Efficiency	32.8
Average Discharge Burnup (GWd/MTU)	Variable
Initial U-235 Enrichment (wt. %)	Variable
Mine Grade (% U)	1.0
Tail Assay (% U-235)	0.3

6.2.2 Reprocessing - Partitioning/Separation

The computational model representing the reprocessing process is designed to track the material streams while accounting for radioactive decay and material losses accrued during the procedure. The material tracks are modeled according to the URanium EXtraction (UREX) process in which the Uranium and Technetium are separated from each other and the other FPs and actinides. A suite of UREX+ processes offer the ability to produce different product lines with varying mixtures of actinides and FPS. The process used for the NES model is UREX+1a which has five product lines made up of: 1) Uranium, 2) Technetium, 3) Cesium/Strontium, 4) TRU, and 5) remaining FPs. In addition to tracking materials the model creates a database for storing material compositions for varying AP1000 input parameters making them easily assessable for analysis.

At the current time (year 1) the reprocessing model is being developed. The numerical computing environment MATLAB® is utilized for the simulation procedure and material database storage.

6.2.3 High Level Waste Storage Facility

The HLW model is still in development. It will simulate a geological repository by tracking isotopic compositions over long periods of time and calculating resulting heat load and dose measurements in order to analyze waste management strategies.

6.3 Integrated Model

The integrated model portion of the study will be finalized in year 2 of the project. Preliminary analysis shows promising potential for a Simulink® model that connects the reactor units and fuel cycle components in a manner that allows UQ and optimization procedures in a realistic and time efficient manner.

7 Preliminary Results

Results for year-one of the project include reactor physics analysis for the AP1000, VHTR, and HEST, with coupled AP1000 – VHTR system analysis. Depletion calculations and material composition results for LEU fueled AP1000 and VHTR are presented. Burnup calculations for TRU-fueled configurations of the VHTR were performed and preliminary results for LEU-fueled HEST are reported.

7.1 AP1000

7.1.1 Neutronic Analysis

The AP1000 model as presented in section 6.1.1 was utilized for all analysis. The results were obtained using the MCNPX code system. The reference core has an average fuel enrichment of 3.39 wt.% and uses a single batch fuel management scheme. The ENDF B-VII cross section library was used for fuel temperatures at 900K and moderator temperatures at 600K. Depletion calculations were performed using 100 day intervals and 700,000 neutron histories per interval.

Figure 7.1 shows the time evolution of the AP1000 core k-effective determined by MCNPX. The core has an initial k-effective value of 1.17. An initial short time step was incorporated to show the neutron poison effect from FPs introduction into the fuel elements at reactor startup. Early on, between the burnup levels of less than 1 GWd/MTU to about 6 GWd/MTU the k-effective increases to a maximum value of approximately 1.19, after which it continually decreases. The initial increase in k-effective is caused by the PYREX rods and IFBA rods that are present in the core. At Beginning of Cycle (BOC) the boron in the PYREX and IFBA rods acts as a strong neutron poison and depresses the reactivity of the core, but as time progresses the boron is depleted, which is evident by the increase in k-effective. The core was burnt to a level of 60 GWd/MTU at which point it is subcritical. At about 28 GWd/MTU the core changes from critical to subcritical. For a single batch core this result is as expected. By incorporating an appropriate fuel shuffling scheme average fuel burnup levels of 60 GWd/MTU can be reached.

The profile of the average neutron flux in the fuel at the BOC is provided in Figure 7.2 for the three different fuel enrichments. Comparing the spectrum profiles the most noticeable difference is the thermal peak. The fuel enriched at 2.35% has the largest thermal peak. The cause of this has to do with the thermal neutron fission cross sections for U-235 being much greater than the radiative capture cross sections for U-238 in the same energy range. Along with the fact that a change in the U-235 enrichment is much more noticeable considering it is present at such a small fraction compared to U-238. Thus, as the percentage of U-235 is decreased from 4.45% to 3.4% to 2.35% less thermal neutrons are removed from the system by neutron absorption (fission and capture) reactions and this is evident by the increase in the thermal peak. Less noticeable is the difference in the fast peak which slightly increases as the enrichment increases, due to the higher rate of fission events which in turn produce more high energy neutrons. The spectrum profiles are as expected for typical PWR cores.

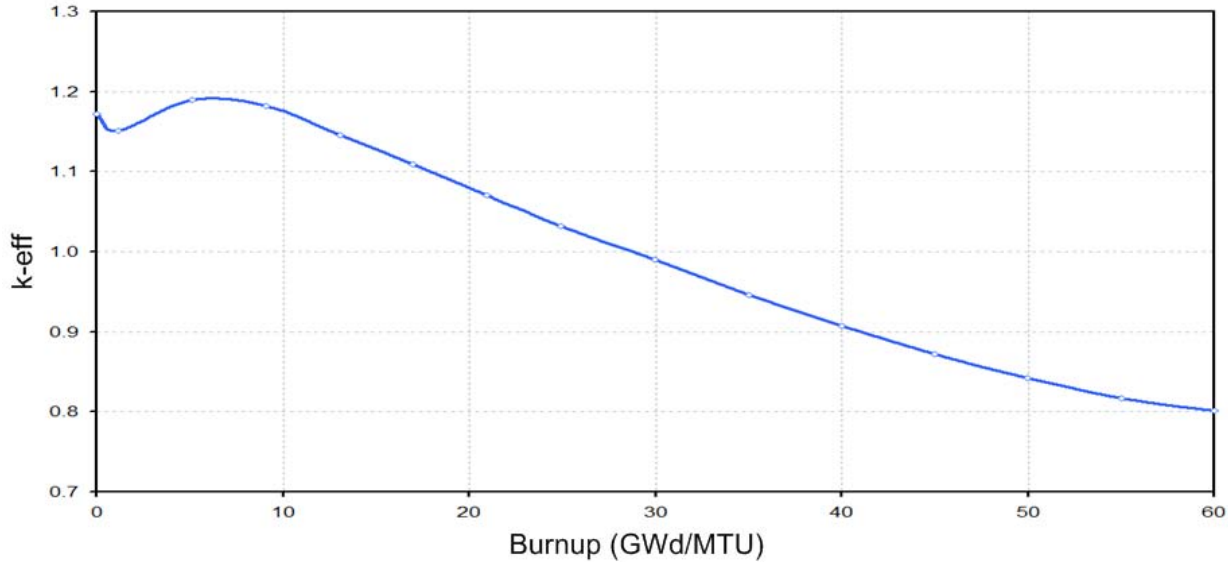

Figure 7.1. AP1000 Whole Core Depletion with MCNPX Code.

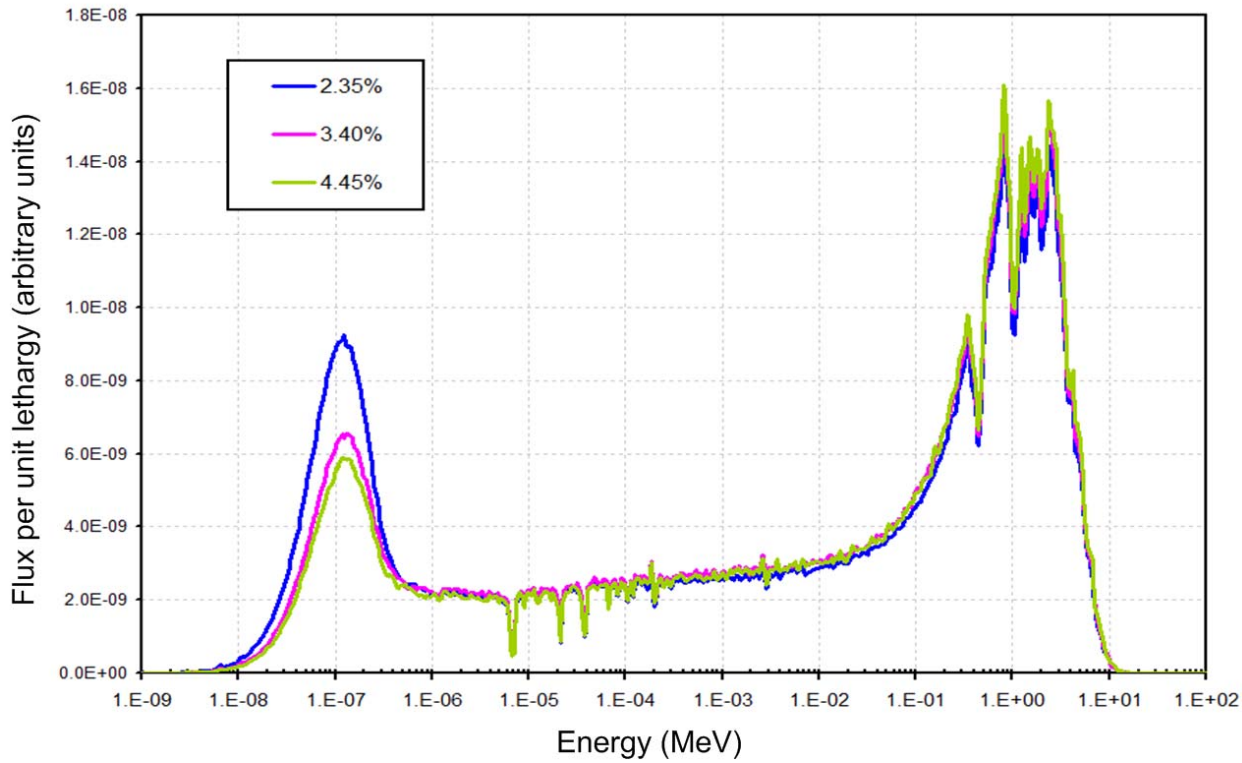

Figure 7.2. AP1000 Fuel Rod Spectra for Different Fuel Enrichments.

The core is loaded with 86.1 Metric Ton Heavy metal (MTU) at BOC. From the time of reactor startup until the End of Cycle (EOC) the fissile component U-235 is depleted but other fissile components are produced when U-238 is transmuted to higher actinides, particularly Pu-239 and Pu-241. Initially the criticality of the core is maintained by U-235 alone, whereas towards the EOC the criticality is mostly maintained by the fission of Pu-239 and Pu-241. Figure 7.3 shows the time evolution of important isotopes within the core, from which a comparison can be made between the consumption of the fuel and the production of important plutonium isotopes. Pu-240 is included because it has a high rate of spontaneous fission, which has important implications regarding inherent proliferation resistance for used fuel.

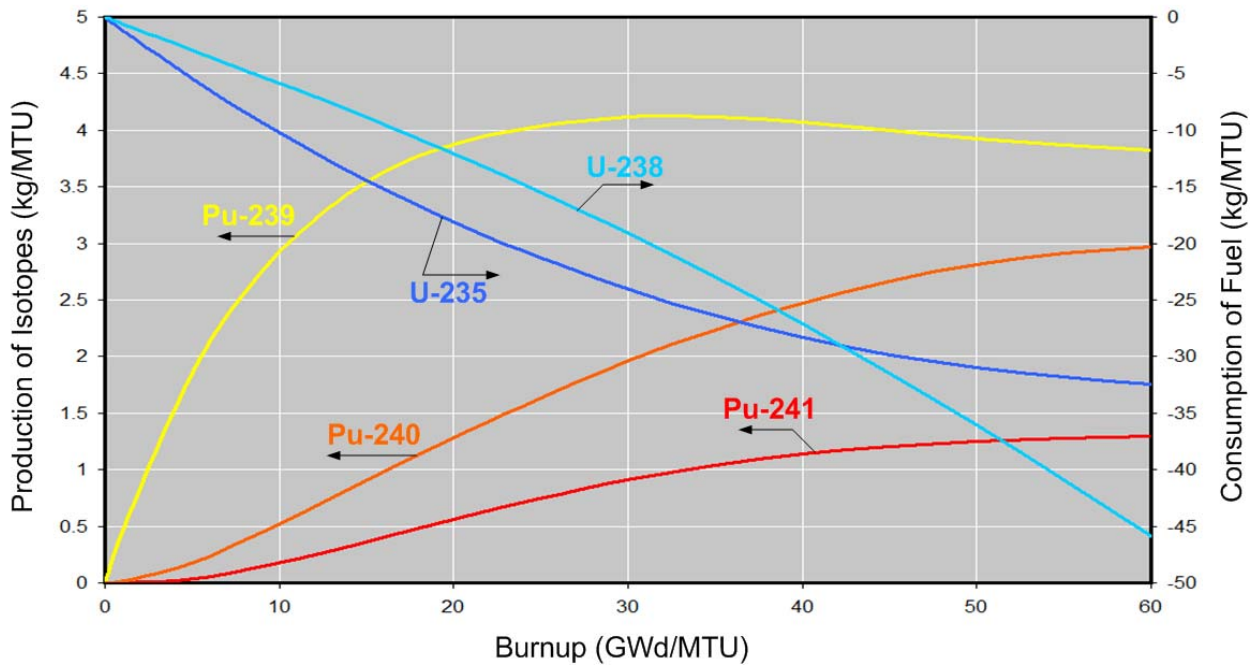

Figure 7.3. AP1000 Production and Consumption of Higher Isotopes in Reference Core.

A more complete tabulation of the actinide transformations within the core is provided in Table 7.1. The mass is given for the actinides produced and consumed at various burnup levels. At a burnup level of about 40 GWd/MTU the amount of U-235 is about the same as the combined amount of Pu-239 and Pu-241 in the core.

Of high importance are the isotopic compositions of the TRUs produced in the core as they will become the fuel component for the VHTR. The used fuel is very "hot" immediately after removal and must be stored in the onsite reactor cooling pool before transportation. Additional storage time is also needed before aqueous reprocessing can be performed. The reprocessing and fuel fabrication procedures will also involve substantial amounts of time. This translates to a decay/cool-down time accounting for the period between fuel removal from the AP1000 up to the time the recycled fuel is ready to be loading into the VHTR.

Table 7.1. Nuclide Masses in the AP100 at Different Burnup Levels.

		Average Fuel Burnup (GWd/MTU)									
		0	20	25	30	35	40	45	50	55	60
Mass (kg/core)	U-234	0.00	0.09	0.10	0.12	0.14	0.16	0.18	0.20	0.23	0.26
	U-235	2920	1309.00	1092.00	851.80	646.00	481.30	349.40	251.50	179.40	127.20
	U-236	0.00	272.20	305.30	340.20	367.70	387.20	399.90	406.30	407.50	405.10
	U-237	0.00	0.54	0.60	0.66	0.75	0.82	0.87	0.92	0.96	0.98
	U-238	83140	82050	81810	81500	81160	80810	80430	80040	79620	79190
	Np-237	0.00	15.08	19.26	24.52	30.03	35.18	40.02	44.28	48.04	51.10
	Pu-238	0.00	2.51	3.86	6.11	8.87	12.04	15.48	18.96	22.36	25.49
	Pu-239	0.00	337.20	347.10	354.20	354.30	350.10	344.30	337.80	333.20	329.10
	Pu-240	0.00	116.40	139.90	168.10	192.30	212.70	229.20	241.80	250.60	255.70
	Pu-241	0.00	51.52	64.46	78.26	89.64	97.80	103.70	107.20	109.70	111.80
	Pu-242	0.00	12.23	19.28	30.83	44.67	60.54	78.38	97.05	116.50	135.70
	Am-241	0.00	0.87	1.23	1.66	2.03	2.28	2.42	2.48	2.50	2.50
	Am-242m	0.00	0.00	0.01	0.01	0.01	0.01	0.01	0.01	0.01	0.01
	Am-243	0.00	1.17	2.21	4.26	7.07	10.67	14.83	19.71	24.83	30.13
	Cm-242	0.00	0.24	0.41	0.69	1.00	1.35	1.67	1.94	2.14	2.28
	Cm-243	0.00	0.00	0.01	0.01	0.02	0.03	0.04	0.05	0.06	0.07
	Cm-244	0.00	0.21	0.50	1.24	2.57	4.73	7.96	12.44	18.40	25.57
	Cm-245	0.00	0.01	0.02	0.05	0.11	0.22	0.40	0.66	1.01	1.44

Table 7.2 provides the isotopic compositions for the TRUs produced at a burnup level of 40 GWd/MTU for a range of decay times. For thermal spectrum systems Pu-239 and Pu-241 are important because they are fissile isotopes. The decay chain and long half life (2.41E4 yrs) for Pu-239 cause it stay at a stable rate for the time range, but Pu-241 has a shorter half life (14.4 yrs) and decreases noticeably. Am-241 and Np-237 demonstrate neutronic properties that classify them as burnable poisons in thermal systems. The long half life (2.14E6 yrs) of Np-237 makes it stable during the decay time, but the long half life (433 yrs) and decay chain (beta-decay of Pu-241) for Am-241 cause it to increase significantly over the 15 year period. The remaining TRU isotopes are considered neutron absorbers with very low fission probability in thermal spectrums, but none of these change much over the given time period. The combination of the decrease in Pu-241 and increase in Am-241 means that extended periods of decay time can have a negative impact on the neutronic properties (e.g. difficulty achieving and/or maintaining criticality) of the recycled TRU when considered as a fuel component for thermal spectrum systems such as the VHTR.

Table 7.2. AP1000 TRU Vectors at 40 GWd/MTU.

Isotope		Decay/Cool-Down Time (yrs)			
		0	5	10	15
weight %	Np-237	4.5447	4.5744	4.6100	4.6594
	Pu-238	1.5471	1.6377	1.5759	1.5164
	Pu-239	44.5706	44.8213	44.8478	44.8848
	Pu-240	27.3478	26.9155	27.0149	27.0878
	Pu-241	12.5133	9.6428	7.5821	5.9606
	Pu-242	7.8256	7.6766	7.6833	7.6897
	Am-241	0.2916	2.9051	4.9451	6.5302
	Am-242m	0.0015	0.0014	0.0014	0.0014
	Am-243	1.3564	1.3319	1.3318	1.3329
	Cm-244	0.0014	0.4932	0.4076	0.3370

7.2 VHTR

7.2.1 Neutronic Analysis: LEU Fuel

The VHTR model as presented in section 6.1.2 was utilized for all analysis. The results were obtained using the MCNP5/MCNPX code system. The reference core has a U-235 fuel enrichment of 8.0 wt.% and uses a single batch fuel management scheme. The ENDF B-VII cross section library was used for an averaged core temperature of 1200K. Depletion calculations were performed using 100 day intervals and 500,000 neutron histories per interval.

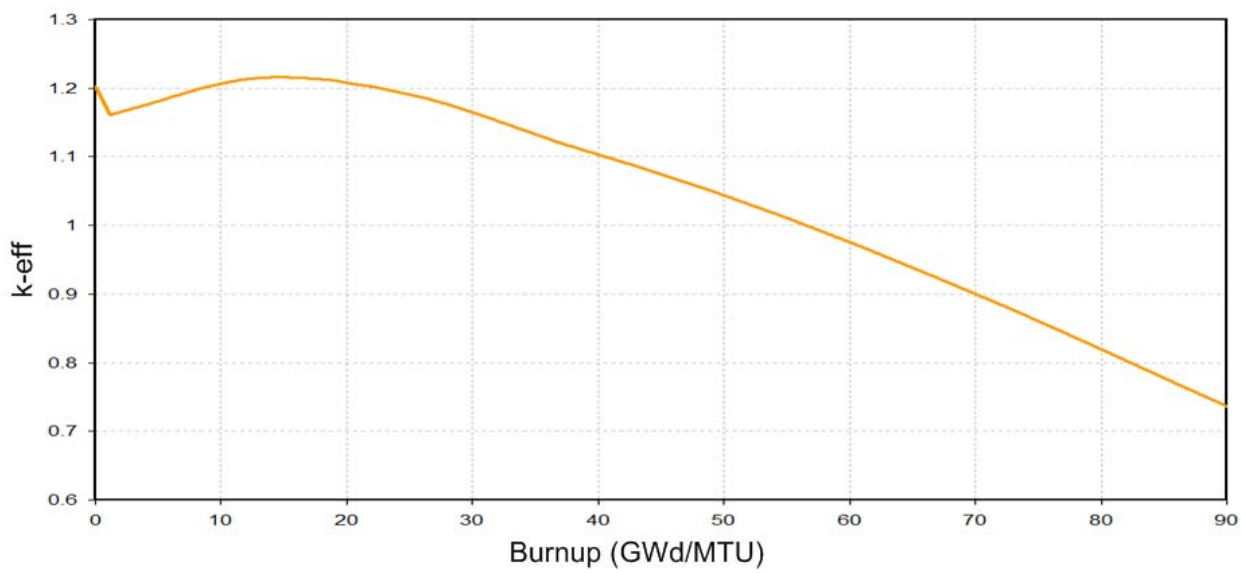

Figure 7.4. Reactivity of LEU-Fueled VHTR.

Figure 7.4 shows the change of the core k-effective as a function of fuel burnup. The core has an initial k-effective value of 1.20. An initial short time step was incorporated to show the neutron poison effect from FPs introduction into the fuel elements at reactor startup. Due to the burnable poison rods present in the core the k-effective increases in the early part of the cycle, between burnup levels 1 - 15 GWd/MTU, then it reaches a maximum of approximately 1.21, after which it continually decreases. The core was burnt to a level of 90 GWd/MTU at which point it is very subcritical. At about 55 GWd/MTU the core changes from critical to subcritical.

The flux profile for different core levels is provided in Figure 7.5. The fuel particle and fuel compact produce similar profiles. The somewhat larger thermal peak and smaller fast peak in the fuel block spectrum signify the additional neutron moderation due to the graphite prismatic fuel block. The same effect is even more pronounced as the average flux for the core is taken into consideration.

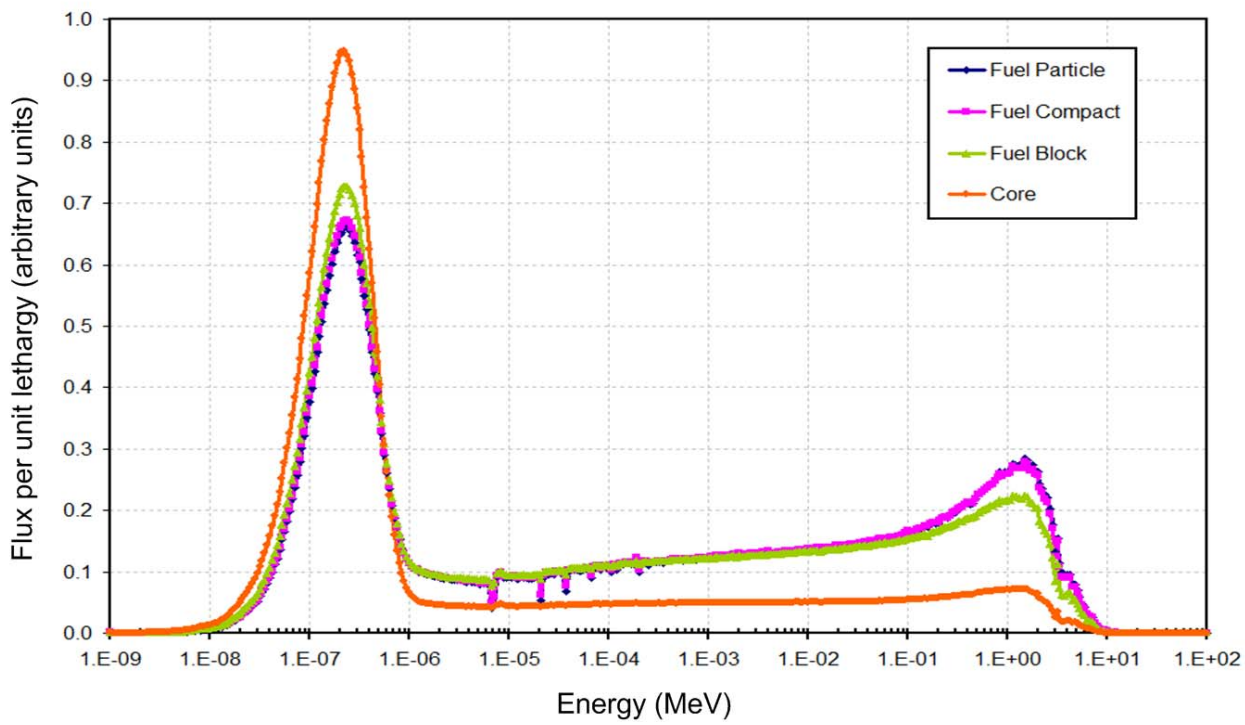

Figure 7.5. LEU-Fueled VHTR Spectra for Core Regions.

A tabulation of the actinide transformations within the core is provided in Table 7.3. The mass is given for the actinides produced and consumed at various burnup levels. Figure 7.6 shows the time evolution of important isotopes within the core. A quick comparison between the normalized production and consumption rates for the AP1000 and VHTR, Figure 7.3 and Figure 7.6, indicate similar trends. The main differences being: 1) the faster rate of depletion of U-235 in the VHTR due to its higher enrichment and 2) the initial steep rate of production of Pu-239 and then its subsequent increased rate of depletion in the VHTR.

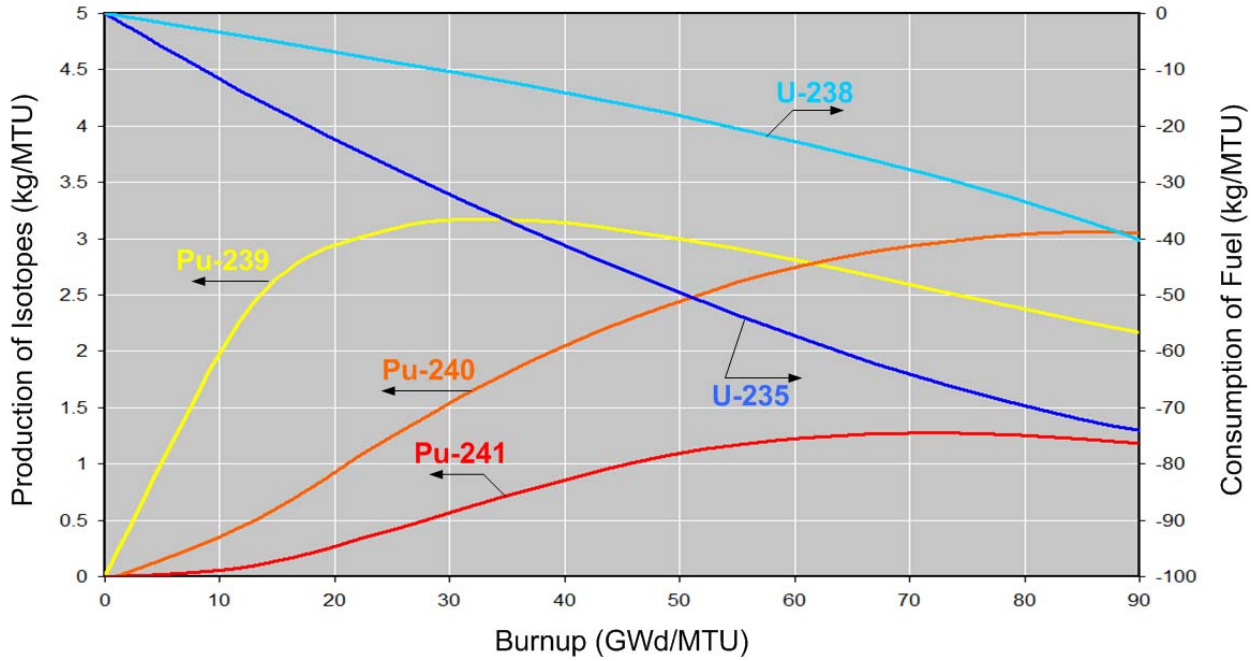

Figure 7.6. Production and Consumption of Higher Isotopes in LEU-Fueled VHTR.

Table 7.3 Nuclide Masses in the LEU-Fueled VHTR at Different Burnup Levels.

		Average Fuel Burnup (GWd/MTU)					
		0	25	37	49	61	73
Mass (kg/core)	U-234	0.0	0.001	0.002	0.002	0.003	0.005
	U-235	401.9	264.40	208.10	156.80	110.90	71.55
	U-236	0.0	23.710	32.960	41.070	47.970	53.440
	U-237	0.0	0.038	0.055	0.073	0.091	0.113
	U-238	4622.0	4579.0	4557.0	4533.0	4506.0	4475.0
	Np-237	0.0	0.391	0.785	1.272	1.808	2.356
	Pu-238	0.0	0.036	0.114	0.266	0.514	0.872
	Pu-239	0.0	15.510	15.900	15.150	14.030	12.700
	Pu-240	0.0	6.264	9.593	12.110	13.880	14.910
	Pu-241	0.0	2.074	3.886	5.382	6.209	6.414
	Pu-242	0.0	0.303	1.038	2.355	4.285	6.798
	Am-241	0.0	0.0132	0.0335	0.0530	0.0620	0.0580
	Am-242m	0.0	0.0001	0.0002	0.0003	0.0003	0.0003
	Am-243	0.0	0.0076	0.0490	0.1620	0.3811	0.7607
	Cm-242	0.0	0.0030	0.0140	0.0356	0.0651	0.0953
	Cm-243	0.0	0.0000	0.0001	0.0003	0.0008	0.0016
	Cm-244	0.0	0.0004	0.0045	0.0229	0.0782	0.2115
	Cm-245	0.0	0.0000	0.0001	0.0005	0.0020	0.0062

7.3 AP1000 - VHTR

7.3.1 Neutronic Analysis: TRU Fuel

The results presented below focus on the performance of the VHTR fueled with the recycled TRUs arising from the AP1000 used fuel. Countless possibilities exist for the isotopic composition of the TRUs as they are dependent on control parameters for the AP1000. The reference case uses the AP1000 model with an average fuel enrichment of 3.49 wt.%, burnup of 40 GWd/MTU, power fraction of 100%, and decay time of 7 years. The resulting TRU composition is listed in Table 7.4.

Table 7.4 Fuel Composition for the TRU-Fueled VHTR.

Nuclide	Mass (kg)	Weigth %
Np-237	229.00	4.545
Pu-238	80.65	1.601
Pu-239	2269.00	45.038
Pu-240	1357.00	26.936
Pu-241	440.40	8.742
Pu-242	381.30	7.569
Am-241	190.10	3.773
Am-242m	0.07	0.001
Am-243	67.42	1.338
Cm-244	23.02	0.457
Total	5037.96	100.000

As the case in the previous section, the flux profile for different core levels is provided in Figure 7.7. Compared to the LEU-fueled VHTR there is a very noticeable difference in the thermal region of the flux profiles. The thermal peak is almost completely depressed in the fuel particle and compact, but more distinguishable in the fuel block. The large thermal absorption cross sections for Am-231 and Pu-240 in particular, but also Np-237 and Pu-242 work together to remove a large portion (as compared to LEU fuel) of the thermal neutrons causing the depressed peak. This effect can have safety implications as the Doppler reactivity coefficient becomes less negative or even possibly positive and can limit TRU fuel loadings. Figure 7.8 is provided for a closer look at just the fuel particle, compact, and block spectra.

Shown in Figure 7.9 is the spectrum for the AP1000 fuel assembly and the spectrum for the VHTR fuel assembly block. As expected, both display flux profiles representative of thermal systems, but the VHTR thermal peak is shifted to slightly higher energies due to the higher core temperature. Also the flux within the VHTR epithermal range is proportionally greater. Overall the VHTR exhibits a harder spectrum making it more efficient at transmuting the higher actinides when compared to the AP1000.

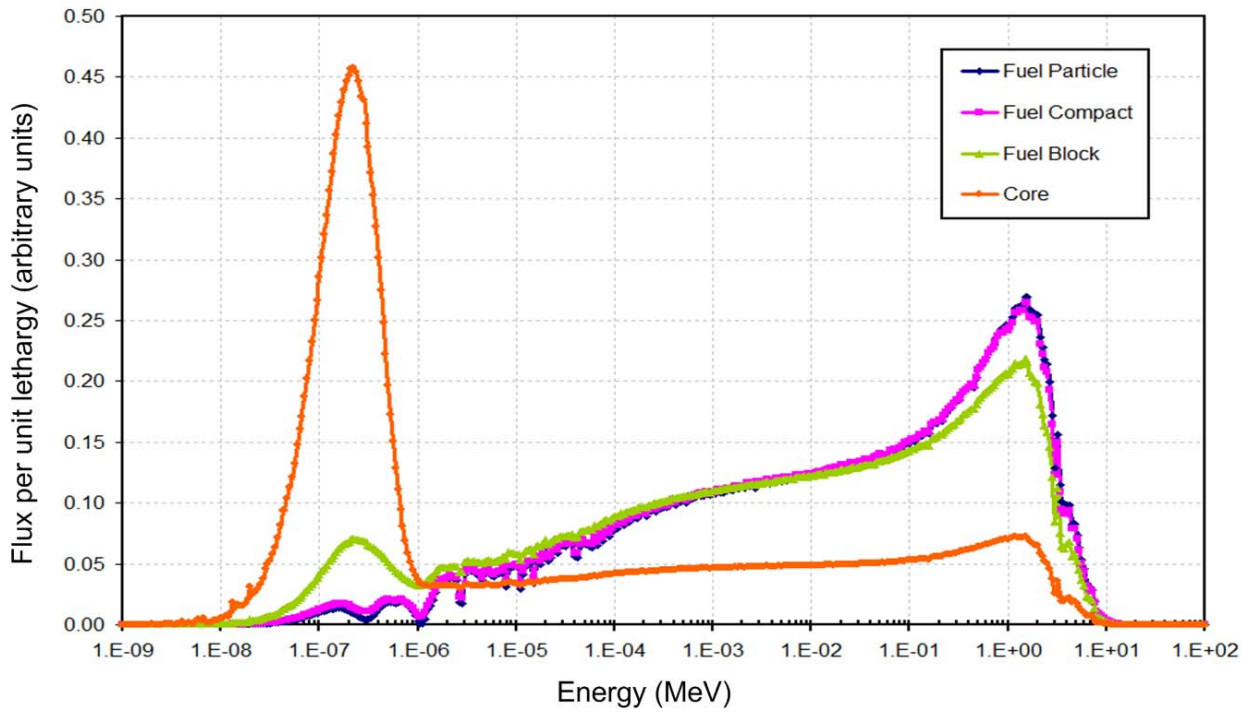

Figure 7.7. TRU-Fueled VHTR Spectra for Core Regions.

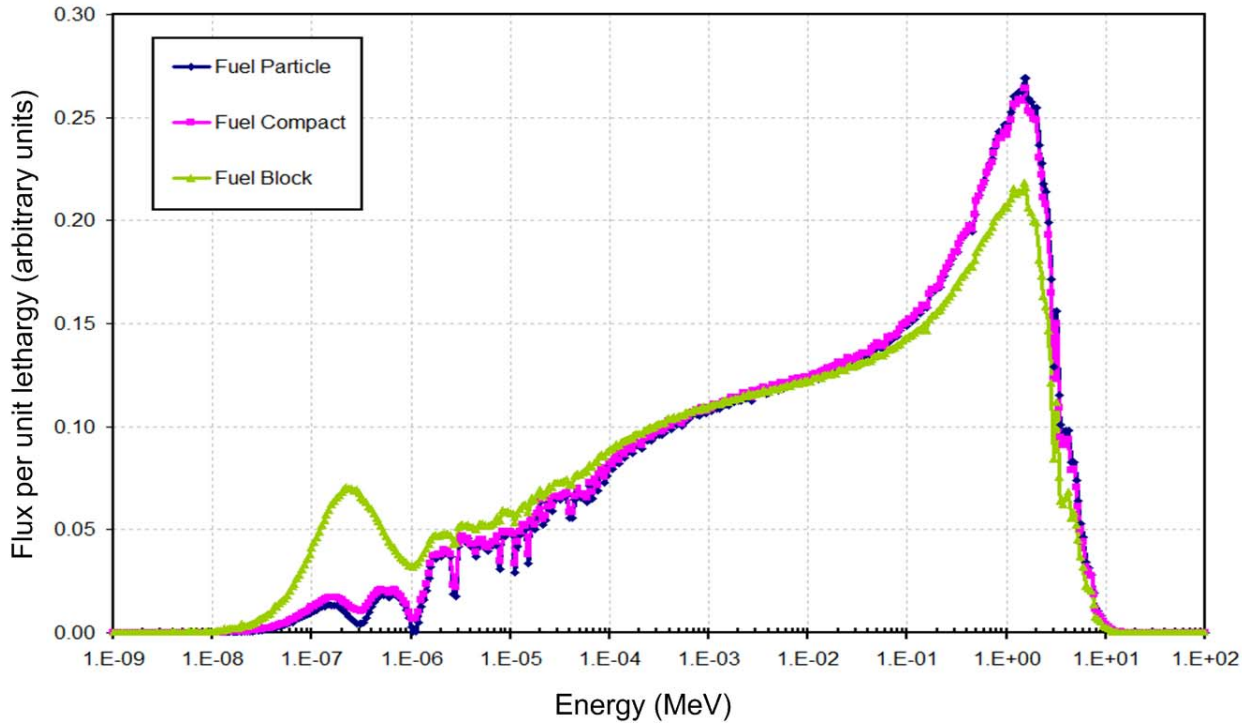

Figure 7.8. TRU-Fueled VHTR Spectra of Particles, Compacts, and Fuel Blocks.

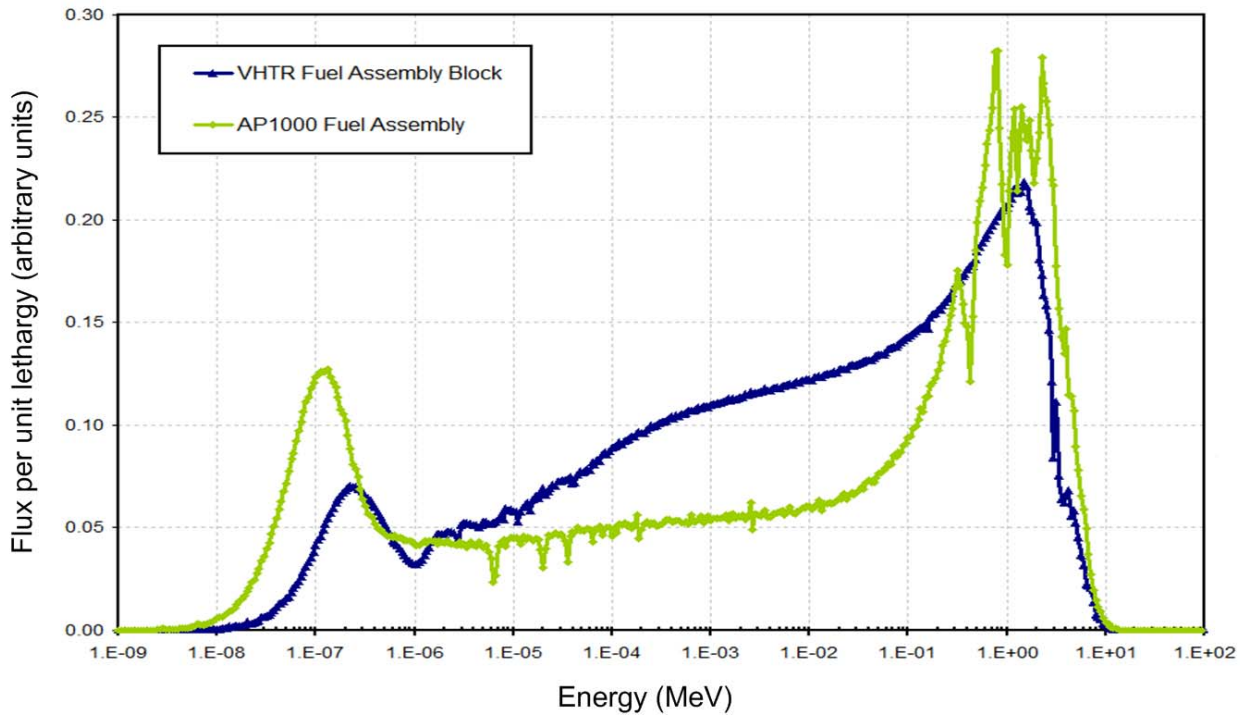

Figure 7.9. TRU-Fueled VHTR and AP1000 Spectra for the Fuel Assemblies.

Figure 7.10 shows the reactivity as a function of the burnup for the TRU-loaded VHTR. It is clear that the reactivity decreases much slower as compared to the LEU-loaded VHTR. This is mainly due to Pu-240 being very efficiently converted into the fissile isotope Pu-241, which is a better fissile fuel than Pu-239 in the VHTR. Additionally, Pu-240 is an effective burnable absorber because of its large cross section, which limits the reactivity swing during the core lifetime. The TRU fueled VHTR maintains criticality up to a burnup level of about 225 GWd/MTU.

The discharge burnup of the reference case for the AP1000 – VHTR system is 218 GWd/MTU and the corresponding cycle length is 1,830 Effective Full Power Days (EFPD). The initial fresh TRU mass for the VHTR is 5,038 kg and the discharge mass is 3,421 kg. The overall consumption of the total heavy metal is 22.2%. The consumption of plutonium is 24.4% including a 54.3% consumption of Pu-239. Am-242m is produced at a high rate, but still makes up only a small fraction of the TRU vector at 0.05%. Table 7.5 includes details for TRU consumption/production during the VHTR core lifetime.

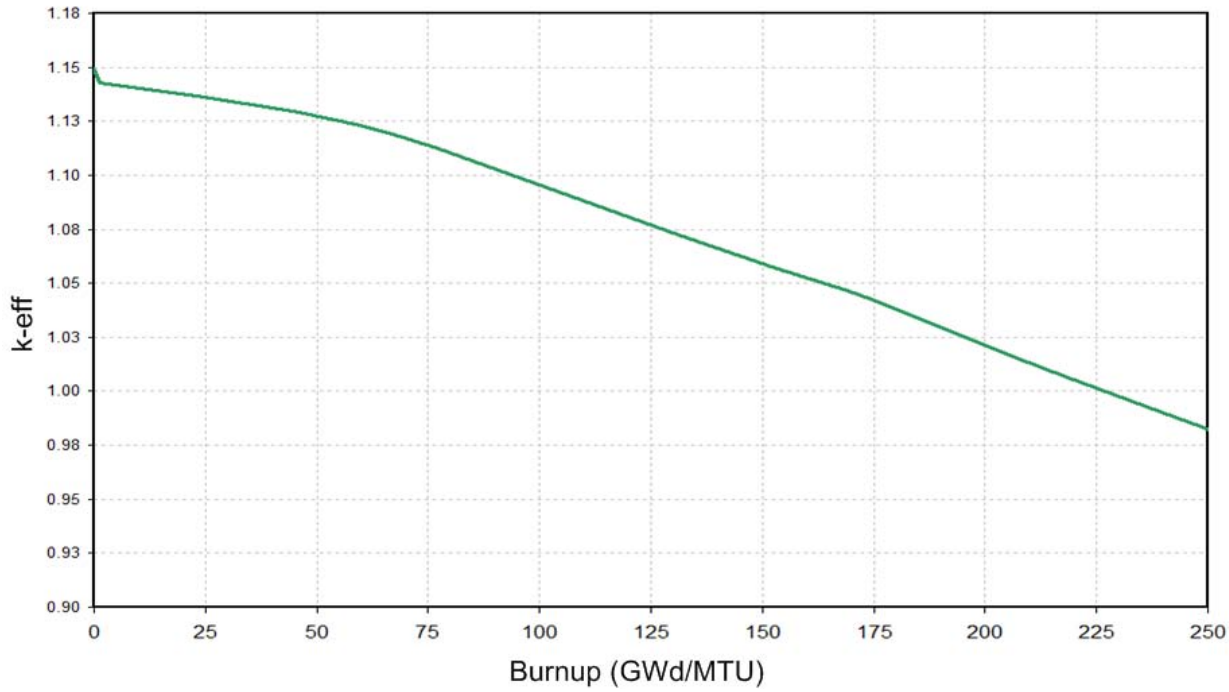

Figure 7.10. Reactivity of TRU-Fueled VHTR.

Table 7.5 Fuel Composition for the TRU-Fueled VHTR.

Nuclide	BOC Intial Loading (kg)	EOC Discharge (kg)	Consumption (%)
U-234	0.00	4.70	
U-235	0.00	1.06	
U-236	0.00	0.68	
Np-237	229.00	146.30	-36.11
Pu-238	80.65	216.70	168.69
Pu-239	2269.00	1037.00	-54.30
Pu-240	1357.00	1303.00	-3.98
Pu-241	440.40	461.40	4.77
Pu-242	381.30	403.30	5.77
Am-241	190.10	151.60	-20.25
Am-242m	0.07	2.15	2941.57
Am-243	67.42	88.39	31.10
Cm-242	0.00	15.36	
Cm-243	0.00	0.78	
Cm-244	23.02	74.22	222.42
Cm-245	0.00	11.65	
Pu	4528.35	3421.40	-24.44
HM	5037.96	3918.29	-22.22

7.4 HEST

Results for HEST are currently limited to neutron spectra analysis for a VHTR fuel assembly block with LEU fuel and centralized 14.1 MeV neutron point source. Future work will include whole core depletion models for analyzing the transmutation potential of VHTR used fuel.

Figure 7.11 shows the neutron flux profile in the single VHTR block with external neutron source. The spectrum has a very sharp peak at 14 MeV and shows little neutron moderation within the system. There is also a smaller, but noticeable peak near 1.5 MeV. This represents the fission peak and indicates a measurable occurrence of fission events within the fuel.

The NES includes three reactor units: the AP1000, VHTR, and HEST. Figure 7.12 shows the neutron spectra for each. The flux profiles are for the reference AP1000, the reference TRU-fueled VHTR, and the preliminary LEU-fueled HEST.

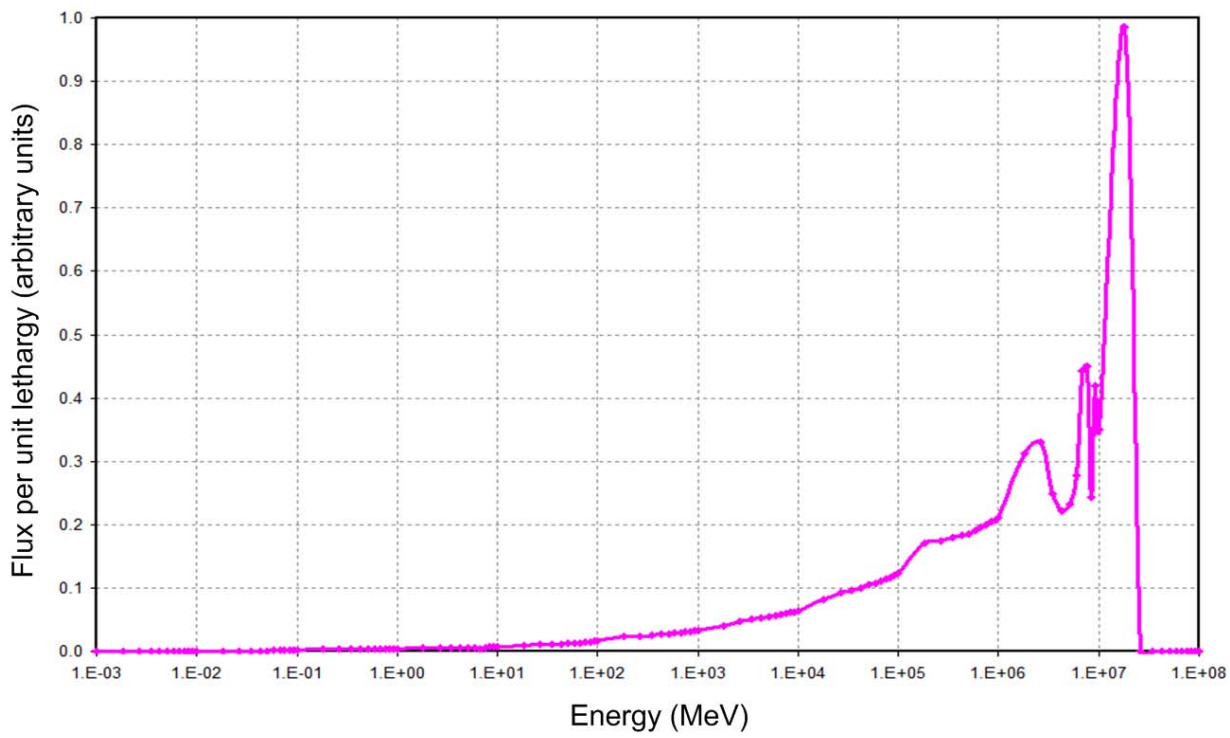

Figure 7.11. HEST Spectrum of the Fuel Block.

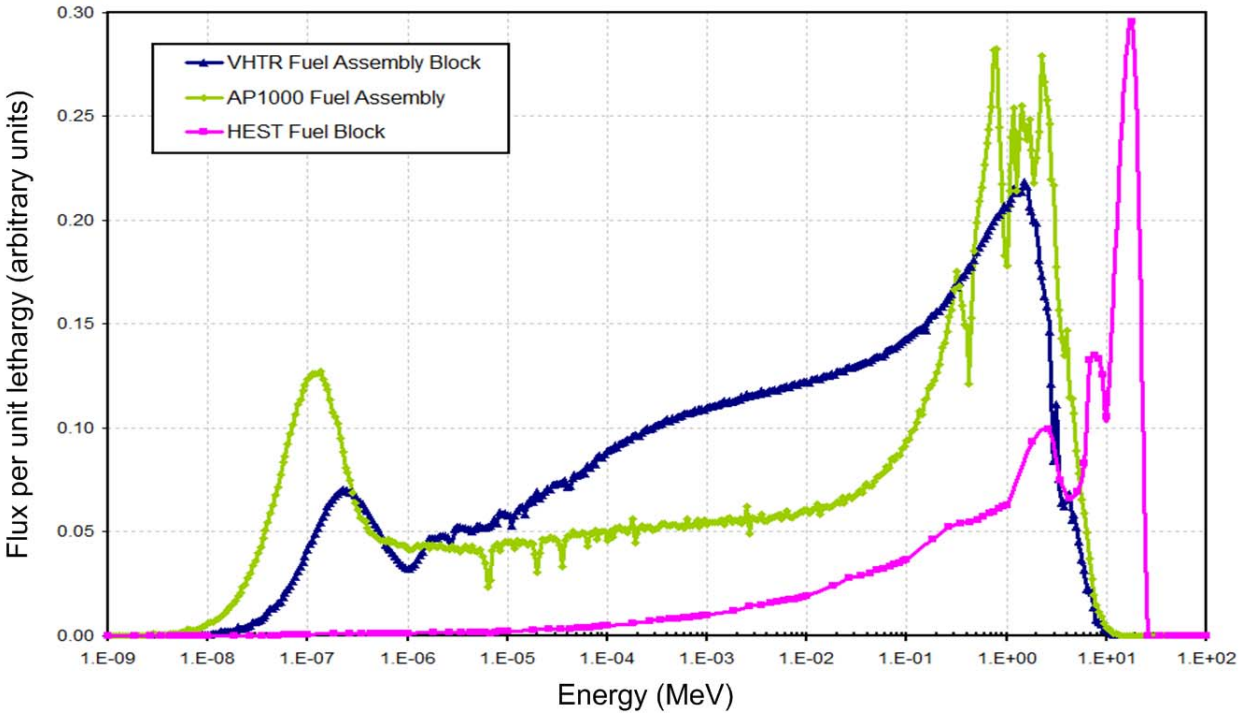

Figure 7.12. HEST, AP1000, and VHTR Spectra Comparison.

8 CONCLUSIONS

The 1st year analysis has shown promise for advanced fuel cycle scenarios that include PWRs, VHTRs and dedicated HEST waste incineration facilities. If deployed, these scenarios may substantially reduce nuclear waste inventories approaching environmentally benign nuclear energy system characteristics. Computational approaches, analysis metrics, and benchmark strategies have been established for future detailed studies.

The AP1000 – VHTR baseline performance indicate an overall TRU destruction of 22.2%. The thermal spectrum system has shown promising results for plutonium destruction. Overall consumption of 24.4% was achieved, with Pu-239 consumption of 54.3%.

The HEST system provides a hard fast spectrum giving it the capability to achieve very high actinide destruction rates in a single pass. All indications thus far signify a successful and timely competition of all the objectives set for the overall project.

8.1 *Future Plans*

The HEST model will be expanded to represent realistic configuration options with fuel loadings derived from the VHTR used fuel. It will also include criticality and depletion calculation capabilities for waste transmutation analysis. The HLW repository model will be further developed and completed. The HEST and repository models will complete the individual modeling needs for the NES.

A system will be developed for integrating the models representing the NES reactor units and fuel cycle components. Plans include creating a material database as produced by each reactor unit and fuel cycle component in the NES. The database will be further populated by varying the control parameters relevant in each case for a predetermined range. A mathematical model will then be developed to access the database and predict NES results for virtually a countless number of possible conditions. This will create an ideal environment for developing and implementing additional methods for performing UQ, optimization, and other related procedures that apply to the NES as a whole and does so without being heavily restricted by Central Processing Unit (CPU) time limitations. Figure 8.1 shows the basic flowchart representing the planned approach for the integrated system.

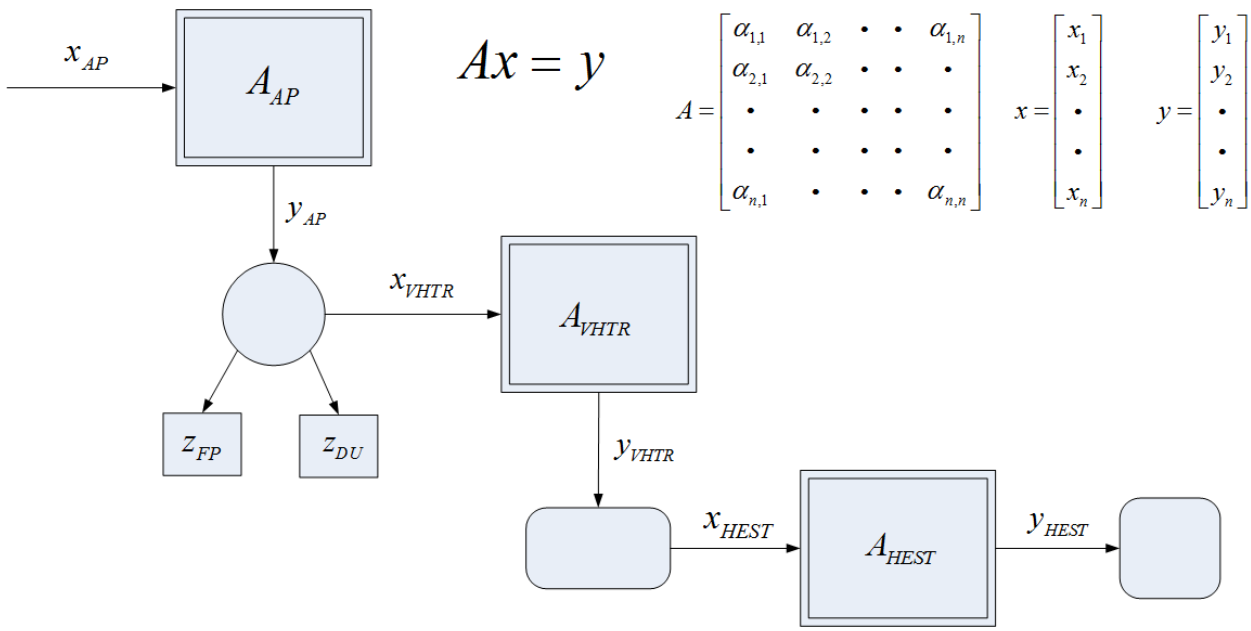

Figure 8.1 **Integrated Model Flowchart.**

9 References

1. Francis M. Vanek, Louis D. Albright, "Energy Systems Engineering: Evaluation and Implementation," McGraw-Hill Professional, United States of America, 17 May 2008.
2. "Human Development Report 2007/2009," Palgrave Macmillan, United Nations Development Program, New York, USA (2007).
3. A.D. Pasternak, Global Energy Futures and Human Development: A Framework for Analysis, Lawrence Livermore National Laboratory, 2000.
4. United Nations. Convention on Climate Change. United Nations. "KYOTO PROTOCOL to the United Nations Framework Convention on Climate Change". 11 Dec. 1997. <http://unfccc.int/resource/docs/convkp/kpeng.html>. 22 Oct. 2006.
5. Paul P. Portney, Robert N. Stavins, "Public Policy for Environmental Protection," RFF Press, 2nd Edition, Washington DC, 4 Aug. 2000.
6. NEA/IAEA, "Uranium 2007: Resources, Production and Demand," OECD, Paris, France, 2008.
7. J.R. Lamarsh, "Introduction to Nuclear Engineering," Addison-Wesley, Massachusetts, USA, 1983.
8. K. Noack, et. al., "The GDT-based fusion neutron source as driver of a minor actinides burner," *Annals of Nuclear Energy* **35**, pp. 1216-1222 (2008).
9. Andrew Taylor, et al., "A route to the brightest possible neutron source," *Science* **315**, pp1092 (2007).
10. T.A. Mehlhorn, B.B. Cipiti, C.L. Olson, G.E. Rochau, "Fusion-fission hybrids for nuclear waste transmutation: A synergistic step between Gen-IV fission and fusion reactors," *Fusion Engineering and Design* **83**, pp 948-953 (2008).
11. A.H. Martinez, Y. Kadi, G. Parks, M. Dahlfors, "Transmutation of nuclear waste in accelerator-driven systems: Fast spectrum," *Annals of Nuclear Energy* **34**, pp. 564-578 (2007).
12. Y. Gohar, T. A. Taiwo, J. E. Cahalan, P. J. Finck, "Assessment of the General Atomics Accelerator Transmutation of Waste Concept Based on the Gas-Turbine Modular Helium Reactor Technology," Technology Development Division, Argonne National Laboratory (2001).
13. W.M. Stacey, et al., "A subcritical, gas-cooled fast transmutation reactor with a fusion neutron source," *Nuclear Technology*, pp. 156-159 (2006).
14. M. Kotschenreuther, P.M. Valanju, S.M. Mahajan, E.A. Schneider, "Fusion-fission transmutation scheme-efficient destruction of nuclear waste," Fusion Engineering and Design **84**, pp. 83-82 (2009)
15. R. BROGLI, R. KRAKOWSKI, "Degree of Sustainability of Various Nuclear Fuel Cycles," LAUR-01-6939, ISSN 1019-0643, Nuclear Energy and Safety Research Department, Paul Scherrer Institute (2002).
16. "The Path to Sustainable Nuclear Energy: Basic and Applied Research Opportunities for Advanced Fuel Cycles", September 2005, Office of Science, U.S. Department of Energy (2005).
17. E. E. Bende, A. H. Hogenbirk, J. L. Kloosterman and H. Van Dam, "Analytical Calculation of the Average Dancoff Factor for a Fuel Kernel in a Pebble-Bed High-Temperature Reactor," *Nuc. Sci. Eng*. **133**, 147-162 (1999).

18. J. Wright, I. Pazsit, “Neutron kinetics in subcritical cores with application to the source modulation method”, *Annals of Nuclear Energy*, **33**, pp. 149–158 (2006).
19. “A Science-Based Case for Large-Scale Simulation”, Vol. 2, September 19, 2004, Office of Science, U.S. Department of Energy (2004).
20. J.S. Hendricks, G.W. McKinney, J.W. Durkee, J.P. Finch, M.L. Fensin, M.R. James, et al., MCNPX, Version 2.6.0, Los Alamos National Laboratory Report LA-UR-08-2216, 2008.
21. “SCALE: A Modular Code System for Performing Standardized Computer Analyses for Licensing Evaluation”, ORNL/TM-2005/39,Ver.5.1, November 3, 2006, Oak Ridge National Laboratory, Tennessee (2006).
22. Westinghouse AP1000 Design Control Documentation Rev. 16 – Tier 2 Chapter 4 – Reactor – Section 4.3 Nuclear Design. ML071580897 (2007-05-26).
23. “Generation IV Nuclear Energy Systems Ten Year Program Plan Volume I”, March 27, 2005, Office of Nuclear Energy, Science, and Technology, USDOE (2005).
24. “Evaluation of High Temperature Gas-cooled Reactor Performance: Benchmark Analysis Related to Initial Testing of the HTTR and HTR-10”, IAEA-TECDOC-1382, International Atomic Energy Agency, Vienna, Austria (2003).
25. D. E. Ames II, P. V. Tsvetkov, “Benchmark Efforts to Support Studies of Advanced VHTRs”, *Proc. 4th Intern. Conf. on HTR Technology (HTR2008)*, Sept. 28 – Oct. 1, 2008, Washington D.C., USA, paper HTR2008-58206, pp. 1 – 8, ASME (2008).
26. S. FEHER and P.F.A. DE LEEGE, "DANCOFF-MC: A Computer Program for Monte Carlo Calculation of Dancoff Factors in Irregular Geometries," IRI-131-95-003 (June 1997).
27. T. A. TAIWO, T. K. KIM, W. S. YANG, and H. S. KHALIL, “Evaluation of High Temperature Gas-Cooled Reactor Physics Experiments as VHTR Benchmark Problems”, ANL-GenIV-059, Argonne National Laboratory, September 2005.
28. Research and Development Report 1953 Facilities for Electronuclear (MTA) Program Report LWS-24736; Status of the MTA Process 1954 Livermore Research Laboratory Report LRL-102.
29. W.B. Lewis, 1952 Report AECL-968.
30. G.A. Bartholomew and P.R. Tunnicliffe, eds. 1966 “The AECL Study for an Intense Neutron-Generator (ING) (technical details)”, Atomic Energy of Canada Limited Report AECL 2600.
31. C.D. Bowman et al., 1992 “Nucl. Istrum. Meth.” A320 366; F. Venneri, et al., Los Alamos Report LA-UR-93-752.
32. Nuclear Fuel Cycle Simulation System (NFCSS), Internal Atomic Energy Agency (2003-2007). http://www-nfcis.iaea.org/NFCSS/NFCSSMain.asp?RightP=Background

10 Appendix A

Author: David Ames
Subject: HTTR Benchmark Description
Date: December 8, 2008

Fuel particle level:

TRISO particle

	material	density (g/cm³)	radius (cm)
Fuel kernel	UO_2	10.41	0.02985
1st coating	PyC	1.14	0.03588
2nd coating	PyC	1.89	0.03895
3rd coating	SiC	3.20	0.04184
4th coating	PyC	1.87	0.04645

Graphite matrix

Material	Density	Impurity
graphite	1.69 g/cm³	0.82 ppm B_{nat}

Unit cell measurements

Volume fraction of grains	Array Pitch	Number of particles per fuel element
0.3	0.1377 cm	176,515

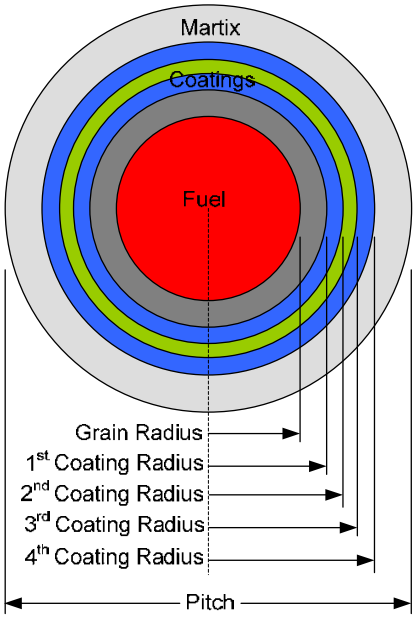

TRISO particle

Fuel element level:

Fuel element properties

Fuel Compact	
Number of fuel particles	176,515
Graphite matrix density	1.690 g/cm³
Graphite matrix Impurity	0.82 ppm B_{nat}
Diameter-inner	1.0 cm
Diameter-outer	2.6 cm
Effective height of fuel rod	54.6 cm

Graphite Sleeve	
Material	Graphite
Density	1.770 g/cm³
Impurity	0.37 ppm B_{nat}
Diameter-inner	2.6 cm
Diameter-outer	3.4 cm
Height	57.7 cm

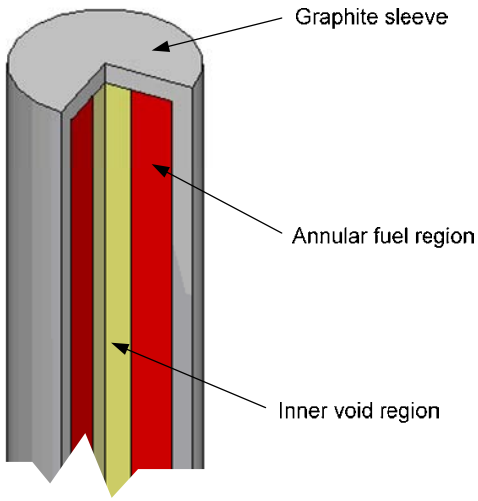

Annular fuel rod

Burnable Poison Rod Properties

Type	H-I	H-II
Absorber section material (2 per rod)	B_4C-C	B_4C-C
Density	1.79 g/cm³	1.82 g/cm³
Natural boron concentration	2.22 wt.%	2.74 wt.%
Diameter	1.39 cm	1.39 cm
Height	20 cm	20 cm
B-10 abundance ratio	18.7 wt.%	18.7 wt.%
Graphite section density	1.77 g/cc	1.77 g/cc
Diameter	1.40 cm	1.40 cm
Height	10 cm	10 cm

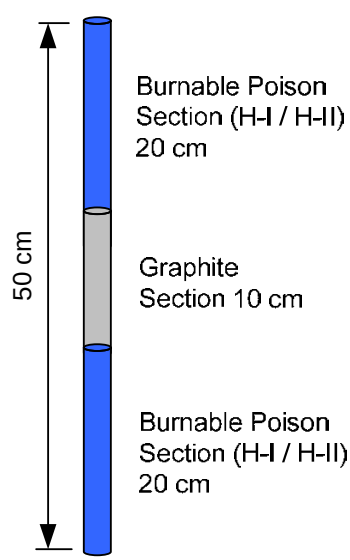

Fuel Assembly Block

Type	Pin-in-block
Configuration	Hexagonal
Material	IG-110 Graphite
Density	1.770 g/cm³
Impurity	0.40 ppm B_{nat}
Height	58.0 cm
Width across the flats	36.0 cm
Number of fuel holes in block	33 or 31
Fuel hole diameter	4.1 cm
Fuel hole height	58.0 cm
Burnable poison holes	3
Burnable poison hole diameter	1.5 cm
Burnable poison hole height	50.0 cm

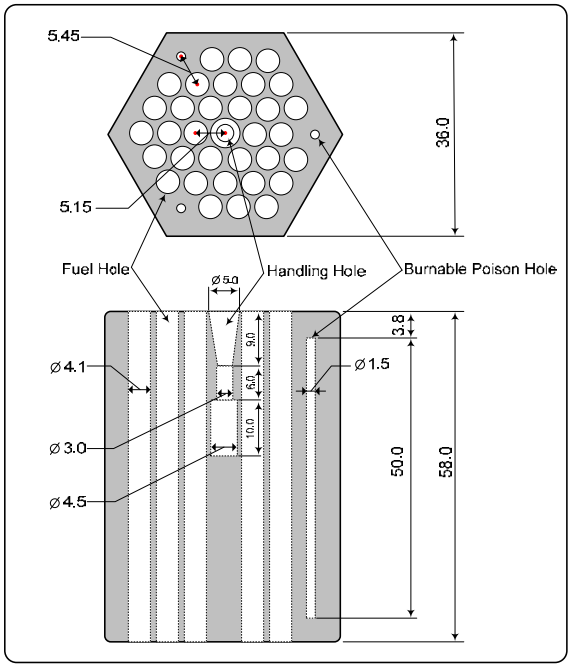

Unit cell measurements

Lattice type	Array Pitch (cm)	Fuel inner radius (cm)	Fuel outer radius (cm)	Sleeve inner radius (cm)	Sleeve outer radius (cm)	Fuel element height (cm)
Triangular	5.15	0.5	1.3	1.3	1.7	54.6

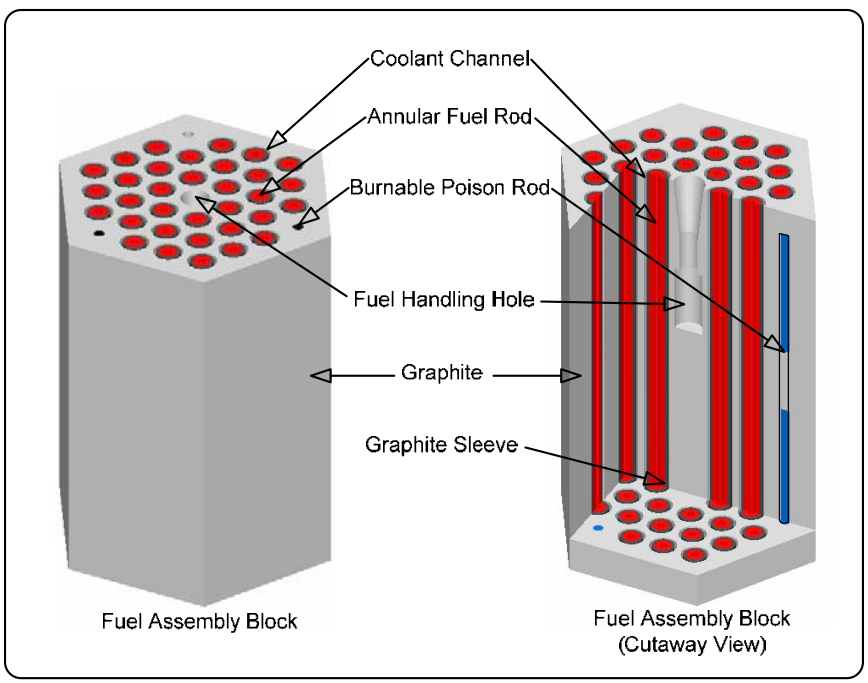

Fuel assembly block with top and quarter section removed to show fuel rods and BP rods.

Control Rod Block and Irradiation Block (irradiation block is identical to control rod block except the holes are used for nuclear instrumentation instead of control rods)

Material	IG-110 Graphite
Density	1.770 g/cm³
Impurity	0.40 ppm B_{nat}
Height	58.0 cm
Width across the flats	36.0 cm
Number control rod holes in block	2
Control rod hole diameter	12.3 cm
Control rod hole height	58.0 cm
Reserve shutdown holes in block	1
Reserve shutdown hole diameter	12.3 cm
Reserve shutdown hole height	58.0 cm

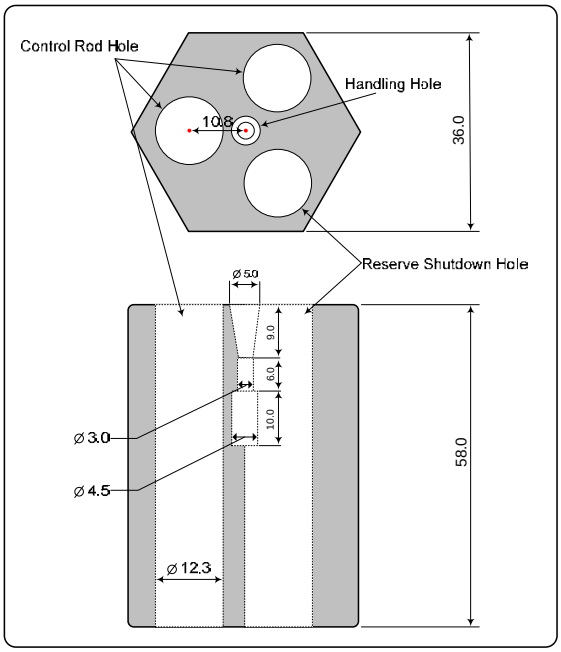

Control Rod Properties

Neutron Absorber Sections (annular)	
Number of neutron absorber sections in each control rod	10
Material	B_4C and C
Density	1.9 g/cm³
Diameter-inner	7.5 cm
Diameter-outer	10.5 cm
Height	29.0 cm
Effective height	290 cm (10 neutron absorber sections)
Spacing between neutron absorber sections	2.2 cm
Control Rod Sleeve	
Material	Alloy 800H
Thickness	0.35 cm
Control Rod	
Number of control rods	32 (16 pairs)
Number of control rods in active core	14 (7 pairs)
Number of control rods in replaceable reflector region	18 (9 pairs)
Diameter-inner	6.5 cm
Diameter-outer	11.3 cm
Height	310 cm

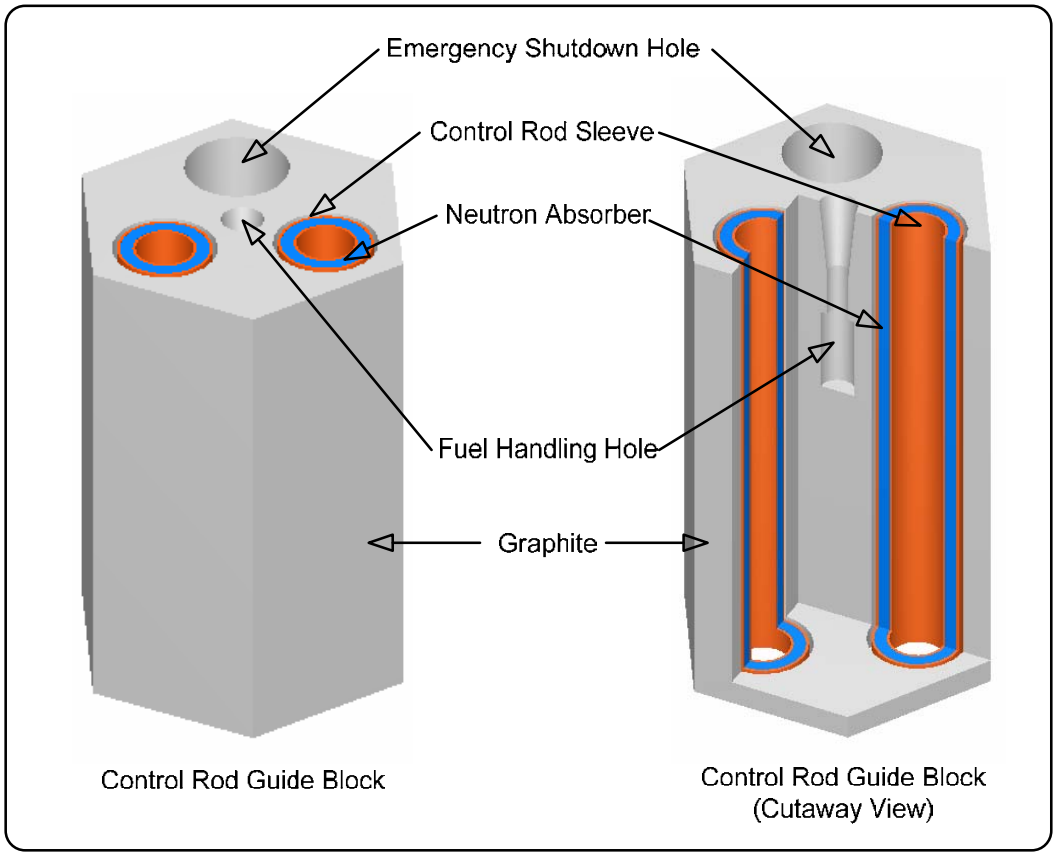

Control rod block with cutaway view

Replaceable Reflector Block (can be solid graphite block or have coolant channels to match the fuel assembly block that it would be associated with)

Configuration	Hexagonal
Material	IG-110 Graphite
Density	1.760 g/cm³
Impurity	0.37 ppm B_{nat}
Height	58.0 cm
Width across the flats	36.0 cm
Coolant channels (if applicable)	33/31
Coolant hole diameter	4.1 cm
Coolant hole height	58.0 cm

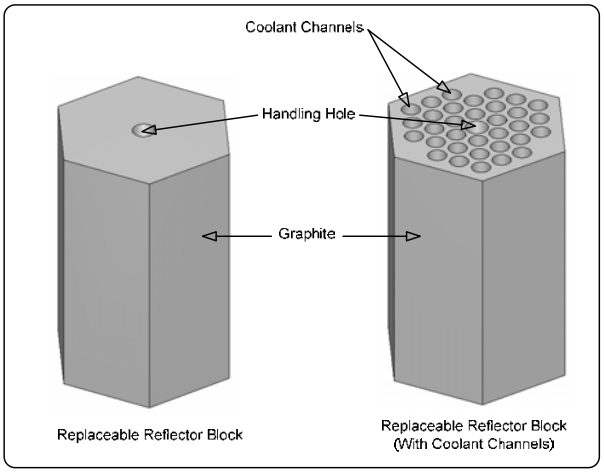

Core Level:

Core Columns

Column	Blocks
Fuel assembly	5 Fuel assembly blocks 4 Reflector blocks (channels)
Reflector	9 Reflector Blocks
Control Rod / Irradiation	9 Control rod blocks

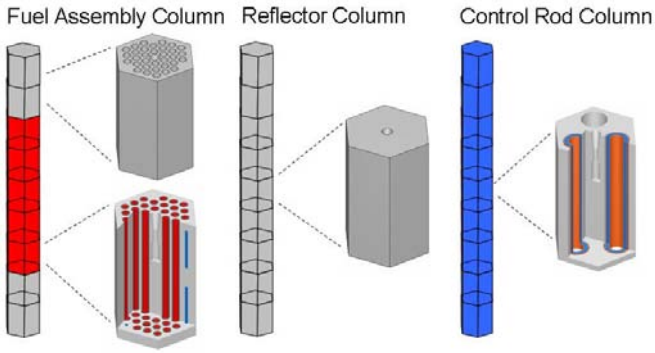

Permanent Reflector Properties

Material	IG-110 Graphite
Density	1.732 g/cm³
Impurity	2 ppm B_{nat}
Height	522 cm
Radius	215 cm

Overall Core Geometry

	Active core	Whole core
Height	290 cm	522 cm
Radius	115 cm (effective)	215 cm

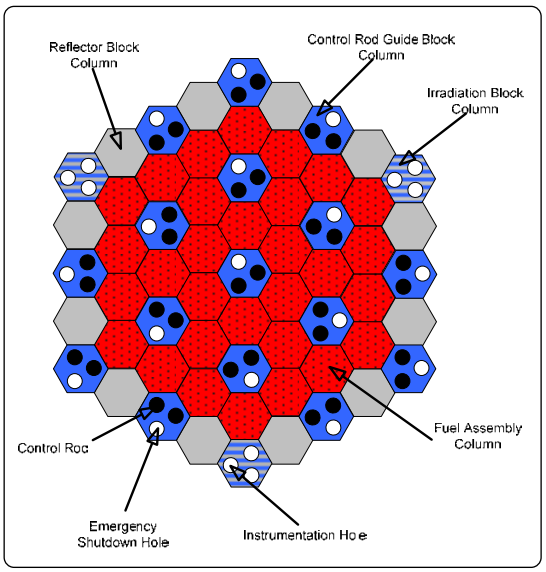

Cross-section core view

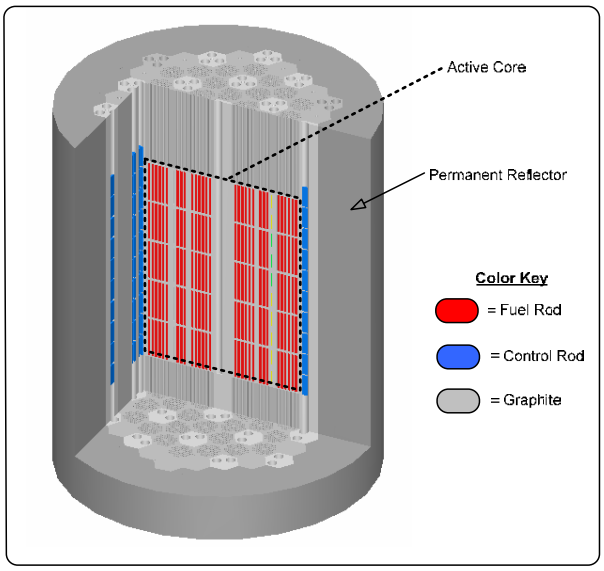

Whole core 3D view

Uranium Enrichments

number	1	2	3	4	5	6	7	8	9	10	11	12
wt. %	3.301	3.864	4.290	4.794	5.162	5.914	6.254	6.681	7.189	7.820	9.358	9.810

Core Arrangement

Layer number from top fuel block	Items	Fuel zone number			
		1	2	3	4
1	Uranium enrichment (wt. %) Number of fuel rods in graphite block Type of burnable poisons	6.681 33 H-I	7.820 33 H-I	9.358 31 H-I	9.810 31 H-I
2	Uranium enrichment (wt. %) Number of fuel rods in graphite block Type of burnable poisons	5.162 33 H-II	6.254 33 H-II	7.189 31 H-II	7.820 31 H-II
3	Uranium enrichment (wt. %) Number of fuel rods in graphite block Type of burnable poisons	4.290 33 H-II	5.162 33 H-II	5.914 31 H-II	6.254 31 H-II
4	Uranium enrichment (wt. %) Number of fuel rods in graphite block Type of burnable poisons	3.301 33 H-I	3.864 33 H-I	4.290 31 H-I	4.794 31 H-I
5	Uranium enrichment (wt. %) Number of fuel rods in graphite block Type of burnable poisons	3.301 33 H-I	3.864 33 H-I	4.290 31 H-I	4.794 31 H-I

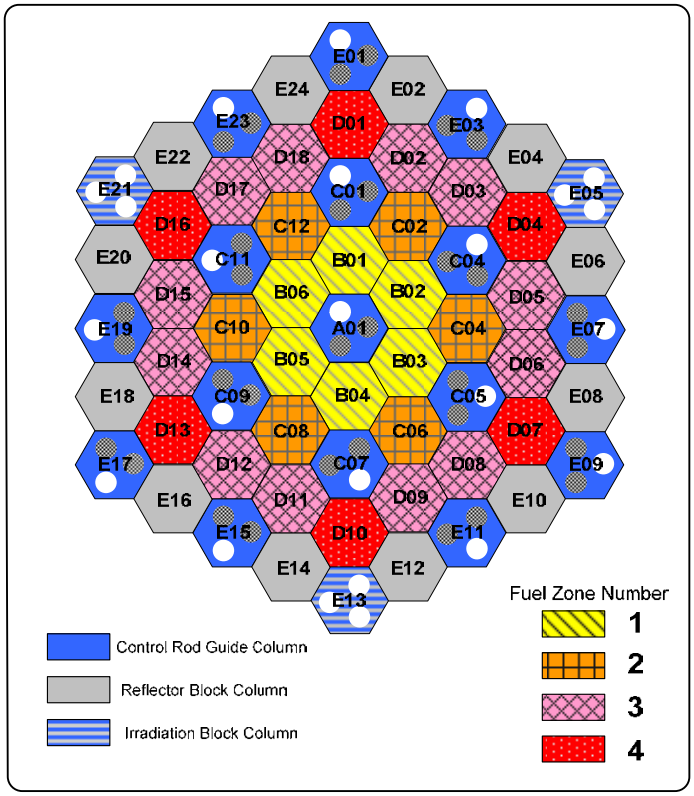

Core Map

Benchmark Results:

Benchmark		VHTR model (calculated)	HTTR (experimental)	Error (%)
Control Rods Fully Withdrawn	k-eff	1.1368 ± 0.0023	1.1363 ± 0.041	0.044
Control Rods Fully Inserted	k-eff	0.6858 ± 0.0019	0.685 ± 0.010	0.117
Critical Insertion Depth (core temperature 300K)	cm	177.1	177.5 ± 0.5	0.225
Critical Insertion Depth (core temperature 418K)	cm	189.9	190.3 ± 0.5	0.210
Temperature Coefficient	dk/k/K	-1.45E-04	-1.42E-04	2.113

ELECTRONIC DISTRIBUTION

Texas A&M University
David Ames II, deames_99@yahoo.com
Ayodeji Alajo, dejialajo@neo.tamu.edu
Raymond Juzaitis, rjuzaitis@tamu.edu
Tom Lewis III, tglewis3@gmail.com
Pavel Tsvetkov, Tsvetkov@tamu.edu

Argonne National Laboratory
Mohamed Gohar, gohar@anl.gov

U.S. Department of Energy
Madeline Feltus, MADELINE.FELTUS@nuclear.energy.gov
Rob Versluis, ROB.VERSLUIS@nuclear.energy.gov

General Atomics
Timothy Bertch, Timothy.Bertch@ga.com
Donald McEachern, Donald.McEachern@ga.com
Arkal Shenoy, Arkal.Shenoy@ga.com

General Electric
Russell Stachowski, Russell.Stachowski@gnf.com

Idaho National Laboratory
Hans Gougar, Hans.Gougar@inl.gov
Kathryn McCarthy, Kathryn.Mccarthy@inl.gov
David Nigg, David.Nigg@inl.gov
Abderrafi Ougouag, Abderrafi.Ougouag@inl.gov

Laurence Livermore National Laboratory
Jeff Latkowski, latkowski@llnl.gov
Ralph Moir, RMoir@Pacbell.net

Logos Technologies
Francesco Venneri, fvenneri@mac.com

Oak Ridge National Laboratory
Mark DeHart, dehartmd@ornl.gov
Jess Gehin, gehinjc@ornl.gov

Sandia National Laboratories
Benjamin Cipiti, bbcipit@sandia.gov
Gary Rochau, gerocha@sandia.gov
Salvador Rodriguez, sbrodri@sandia.gov
D. Chavez, dchavez@sandia.gov

Sandia National Laboratories